Journal of Computational Physics 441 (2021) 110426

Contents lists available at ScienceDirect

Journal of Computational Physics

www.elsevier.com/locate/jcp

A stable FE method for the space-time solution of the Cahn-Hilliard equation

Eirik Valseth [a,*], Albert Romkes [b], Austin R. Kaul [b]

[a] Oden Institute for Computational Engineering and Sciences, The University of Texas at Austin, Austin, TX 78712, USA
[b] Department of Mechanical Engineering, South Dakota School of Mines & Technology, Rapid City, SD 57701, USA

ARTICLE INFO

Article history:
Available online 21 May 2021

Keywords:
Cahn-Hilliard equation
Phase field transition
Discontinuous Petrov-Galerkin and adaptivity

ABSTRACT

In its application to the modeling of a mineral separation process, we propose the numerical analysis of the Cahn-Hilliard equation by employing space-time discretizations of the automatic variationally stable finite element (AVS-FE) method. The AVS-FE method is a Petrov-Galerkin method which employs the concept of optimal discontinuous test functions of the discontinuous Petrov-Galerkin (DPG) method by Demkowicz and Gopalakrishnan. The trial space, however, consists of globally continuous Hilbert spaces such as $H^1(\Omega)$ and $H(\mathrm{div}, \Omega)$. Hence, the AVS-FE approximations employ classical C^0 or Raviart-Thomas FE basis functions. The optimal test functions guarantee the numerical stability of the AVS-FE method and lead to discrete systems that are symmetric and positive definite. Hence, the AVS-FE method can solve the Cahn-Hilliard equation in both space and time without a restrictive CFL condition to dictate the space-time element size. We present multiple numerical verifications of both stationary and transient problems. The verifications show optimal rates of convergence in $L^2(\Omega)$ and $H^1(\Omega)$ norms. Results for mesh adaptive refinements in both space and time using a built-in error estimator of the AVS-FE method are also presented.

1. Introduction

The refinement and concentration of minerals from mineral ores is a process that typically requires the use of water such as flowing film and froth flotation concentrators. Processing facilities in the United States consume large amounts of water, in some cases up to $60,000m^3$ each day [1]. Therefore, sustainable approaches to mineral concentration that significantly reduce or remove the need for water are needed to aid in conservation efforts. Furthermore, the location of several copper mines in the United States is in arid regions of the Southwest, thereby further increasing the importance of conservation efforts. It has been proposed by researchers at South Dakota School of Mines & Technology (SDSM&T) to exploit the adhesion forces between mineral particles and specifically tailored substrates to develop new mineral separation techniques using as little water as possible. Thus, a new type of mineral separator must be developed and designed. To aid in the design process, it is necessary to predict the mineral separation process which requires simulation of the accumulation of mineral particles on chemically treated substrates. This accumulation is to be modeled by the Cahn-Hilliard equation.

The mathematical analysis and well posedness results for the Cahn-Hilliard equation have been established in, e.g., [2] by Elliott and Zheng, thereby setting the stage for the application of a FE method in its approximation. However, there are two

* Corresponding author.
E-mail addresses: Eirik@utexas.edu (E. Valseth), Albert.Romkes@sdsmt.edu (A. Romkes), Austin.Kaul@mines.sdsmt.edu (A.R. Kaul).

https://doi.org/10.1016/j.jcp.2021.110426
0021-9991/

challenges: *i*) the nonlinearity of the Cahn-Hilliard equation and *ii*) the transient nature of this problem leading to a loss of the numerical stability for the Galerkin FE method. The second challenge is typically critical, as FE methods for nonlinear problems have been established successfully in, e.g., [3]. To achieve stability in the classical Galerkin FE method, the FE mesh partition, i.e., element size, must be fine enough to establish numerically stable FE approximations thereby leaving the Galerkin FE method unsuitable for a space-time approximation of the Cahn-Hilliard equation. When solving transient partial differential equations (PDE)s in a FE framework, a method of lines approach is typically taken, i.e., FE methods are employed in the spatial domain whereas the temporal domain is discretized by a finite difference scheme. The numerical stability of finite difference schemes is then established through the Courant-Friedrichs-Lewy (CFL) condition [4]. This approach has been employed by several authors to establish approximations of the Cahn-Hilliard equation using several flavors of FE methods including least squares FE method, discontinuous Galerkin methods, and isogeometric analysis (see [5–11]).

An alternative to temporal discretizations using difference methods and a CFL condition are conditionally stable FE methods which have been successfully applied to transient problems, see, e.g., [12–14]. While these space-time methods have been successful in the FE approximation of transient phenomena, their conditional stability requires arduous a priori analyses to properly determine their stabilization parameters. Guaranteed stable FE methods are also applicable for transient PDEs such as the DPG method [15–17] or least squares FE methods [18]. Fernandino and Dorao [10] applied the least squares FE method successfully to a Cahn-Hilliard problem in both space and time using basis functions that are of higher order continuity than classical Galerkin FE methods. The computational cost of these space-time FE methods is typically higher than the method of lines approach but the FE formulations have the advantage that they can employ a wide range of tools such as *a priori* and *a posteriori* error estimation and *hp*-adaptive refinement strategies in both space and time. Thus, the (potential) additional computational cost can be justified.

The AVS-FE method, introduced by Calo, Romkes, and Valseth in [19], is a stable FE method, i.e., the AVS-FE approximations are guaranteed to remain stable for any PDE as long as the kernel of the underlying differential operator is trivial and the optimal test functions are resolved with sufficient accuracy. This method is a Petrov-Galerkin method in which the trial space consists of globally continuous FE bases and the test space of piecewise discontinuous functions. Hence, it is a hybrid between the DPG method of Demkowicz and Gopalakrishnan [20] and classical Galerkin FE methods. In addition to its discrete stability, other features of the AVS-FE method are highly accurate flux approximations, due to its first-order system setting, and its ability to compute optimal discontinuous test functions on the fly, element-by-element. Other related methods are the first-order system least squares FE method [18] and the method of Calo et al. [21] in which a discretely stable discontinuous Galerkin formulation is used in a minimum residual setting.

In this paper, we develop space-time AVS-FE approximations of the Cahn-Hilliard equation. A space-time AVS-FE method is chosen to exploit its stability property, its convergence properties, and the built-in error indicators allowing us to employ mesh adaptive refinement strategies. The Cahn-Hilliard equation being nonlinear requires special treatment and we take the approach of Carstensen et al. in [22]. To start, we introduce the mineral processing application and the corresponding model Cahn-Hilliard boundary value problem (BVP), in addition to notations and conventions in Section 2. Next, we review the AVS-FE methodology in Section 2.2 for linear problems and introduce the concepts of [22] to be employed to perform nonlinear iterations. In Section 3, we derive the equivalent AVS-FE weak formulation for the Cahn-Hilliard BVP. In Section 4, we perform multiple numerical verifications. First, in Section 4.1, we present verifications for problems with manufactured exact solutions to assess convergence properties under both uniform and adaptive mesh refinements. Then, in Section 4.2, we present a phase separation problem for the Cahn-Hilliard problem from literature that is spatially two dimensional. The last numerical verification we consider is a heuristic model for a mineral separation process to verify the applicability of the Cahn-Hilliard equation to mineral separation. Finally, we conclude with remarks on the results and future works in Section 5.

2. Model problem and review of the AVS-FE method

2.1. Model problem

The Cahn-Hilliard equation [23] was introduced to model the evolution of the phase transition of components in a binary alloy from a mixed to a separated state. The equation is a fourth order nonlinear PDE and can be found in several forms in literature. Here, we consider the following form:

$$-\frac{\partial u}{\partial t} + D\,\Delta\left[u^3 - u - \lambda\,\Delta\,u\right] = 0, \tag{1}$$

where $u = u(\mathbf{x}, t)$ denotes the concentration of a constituent undergoing a phase transition, Δ is the spatial Laplacian, $D \in L^\infty(\Omega)$ is the diffusion coefficient, and $\lambda \in L^\infty(\Omega)$ is the square of the width of the transition region in the separation process. Note that D is of unit $\frac{m^2}{s}$ and $\sqrt{\lambda}$ is of unit m^2.

In collaboration with a team of metallurgists at the SDSM&T, we propose to use the Cahn-Hilliard equation to model a particular mineral separation process. The proposed mineral separation process will exploit the forces of adhesion between mineral particles and substrates, both of which are potentially treated, i.e., functionalized to ensure maximum adhesion of desirable minerals. In Fig. 1, a conceptual sketch of the process is shown. Ore enters the separator in a stream of air, where the desirable minerals adhere to the substrate and the remainder of the ore ends up in what is referred to as tailings. The

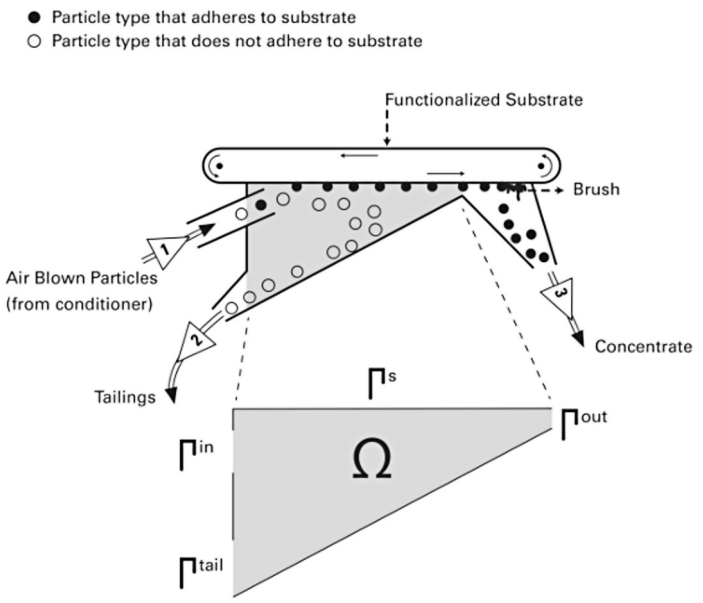

Fig. 1. Conceptual sketch of mineral separator (Courtesy of Brian Hill of University Relations at SDSM&T).

motivation for the development of this type of separation process stems from the fact that it would greatly reduce the use of water compared to currently used techniques. These generally consist of flotation processes which require large amounts of water to establish proper mineral separation from the ore. Now, in the design of the newly proposed separation method, it is necessary to predict the separation of the mineral concentration as it accumulates onto the substrate. To do so, we use the Cahn-Hilliard equation.

In the particular application of the Cahn-Hilliard equation to the mineral separation process, the concentration function $u = u(\mathbf{x}, t)$ represents the mineral concentration at a material point $\mathbf{x}$ and time t. Thus, in the spirit of the original application of this equation, a value $u(\mathbf{x}, t) = 1$ represents the scenario in which the desired mineral has separated from the flow of minerals and has adhered to the substrate. Conversely, a value $u(\mathbf{x}, t) = 0$ denotes the scenario in which the desired mineral particle is still fully dispersed in the flow of minerals. Values between 0 and 1 identify areas in which the mineral particles are in the process of separating.

For the mathematical model of the separation process, we consider only the portion of the mineral separator in which the mineral separation occurs. The boundary, which encloses the separator is assumed to consist of several disjoint portions corresponding to the substrate (onto which the mineral accumulates), the inflow boundary (where the minerals enter the separator), the tailing boundary (where minerals that fail to adhere to the substrate exit the separator), and finally the outflow boundary (where the accumulated minerals exit the separator). Additionally, there may be additional portions of the boundary that serve to encompass the separation process. In Fig. 1, an example mineral separator computational domain Ω is shown.

To establish approximations of the Cahn-Hilliard equation, proper boundary and initial conditions are needed to guarantee physically meaningful results. Let $\Omega \subset \mathbb{R}^2$ be an open bounded domain (see Fig. 1) with Lipschitz boundary $\partial\Omega$ and outward unit normal vector $\mathbf{n}$. Also, let $t = 0$ be the initial time and $t = T$ the final time. The boundary $\partial\Omega$ consists of open subsections:

- Γ_s - the portion of $\partial\Omega$ that coincides with the functionalized substrate upon which mineral accumulation occurs.
- Γ_{in} - the inflow boundary.
- Γ_{out} - the portion of the boundary $\partial\Omega$ through which the accumulated separated mineral exits the separator.
- Γ_{tail} - the outflow boundary, containing the mineral particles that failed to adhere.
- Γ_0 - the remaining portion of the boundary $\partial\Omega$ which contains the entire separation process.

The intersection of these portions is empty and $\partial\Omega = \overline{\Gamma_s \cup \Gamma_{in} \cup \Gamma_{out} \cup \Gamma_{tail} \cup \Gamma_0}$. With the boundary identified by these subsets, the proper boundary conditions for the case of mineral separation are as follows:

- $u = 1$, $\mathbf{x} \in \Gamma_s$, $t \in (0, T)$, i.e., the mineral particles have adhered to the substrate and separated from the flow field.
- $u = 0$, $\mathbf{x} \in \partial\Omega \setminus \Gamma_s$, $t \in (0, T)$, i.e., no mineral particles adhere to the remainder of the separator.
- $u^3 - u - \lambda \Delta u = 0$, $\mathbf{x} \in \partial\Omega$, $t \in (0, T)$, if there is no separation ongoing, the "chemical potential" $u^3 - u - \lambda \Delta u$ must vanish.

Finally, the initial conditions for the mineral separation application are:

- $u = u_{in}$, $\mathbf{x} \in \Gamma_{in}$, $t = 0$, i.e., we assume the separator has no material in it at the onset of the separation process. Hence, the initial conditions are zero on all boundaries.
- $u = 0$, $\mathbf{x} \in \partial\Omega \setminus \Gamma_s$, $t = 0$.
- $u = 0$, $\mathbf{x} \in \Omega$, $t = 0$.

where u_{in} is the concentration of the desired mineral as it enters the separator.

With boundary and initial conditions defined along with the PDE (1), we consider the following Cahn-Hilliard initial boundary value problem (IBVP):

$$\boxed{\begin{aligned} &\text{Find } u \text{ such that:} \\ &-\frac{\partial u}{\partial t} + D\,\Delta\left[u^3 - u - \lambda\,\Delta u\right] = 0, \quad \text{in } \Omega \times (0,T), \\ &u = u_0, \quad \text{on } \partial\Omega, \\ &u = u_{initial}, \quad \text{in } \Omega, \\ &u^3 - u - \lambda\,\Delta u = g, \quad \text{on } \partial\Omega, \end{aligned}} \tag{2}$$

where the values of u_0, $u_{initial}$, and g are as given in the preceding lists. For generality, we keep these arbitrary and employ specific choices in the numerical verifications of Section 4.

While the goal of the current research project is to use the Cahn-Hillard equation as a model problem for mineral separation and the design of a mineral separator, we limit our presentation to the numerical approximation of the Cahn-Hilliard initial boundary value problem (IBVP) on general domains Ω as this is a key stepping stone towards the research goal and the design of the separator is still work in progress.

2.2. Review of the AVS-FE method

The AVS-FE method has been introduced by Calo, Romkes and Valseth in [19]. Attractive features of the AVS-FE method to be exploited for the Cahn-Hilliard problem are its discrete numerical stability property and ease of adaptive mesh refinements due to its built-in error estimator and indicators. The AVS-FE method is a Petrov-Galerkin method in which the trial space consists of continuous FE basis functions, and the test space consists of piecewise discontinuous functions. The discontinuous test space is spanned by so called 'optimal' test functions that are computed on-the-fly by invoking the DPG philosophy [20,24–27].

To introduce the AVS-FE method here, we consider a domain Ω partitioned into elements:

$$\Omega = \text{int}\Big(\bigcup_{K_m \in \mathscr{P}_h} \overline{K_m}\Big), \tag{3}$$

and an abstract AVS-FE weak form in which the underlying differential operator is linear:

$$\boxed{\begin{aligned} &\text{Find } \mathfrak{u} \in U(\Omega) \quad \text{such that:} \\ &B(\mathfrak{u}, \mathfrak{v}) = F(\mathfrak{v}), \quad \forall \mathfrak{v} \in V(\mathscr{P}_h), \end{aligned}} \tag{4}$$

where $\mathfrak{u}$ and $\mathfrak{v}$ are the vector valued trial and test functions, respectively, $U(\Omega)$ is the trial space, $V(\mathscr{P}_h)$ the broken test space, $B : U(\Omega) \times V(\mathscr{P}_h) \longrightarrow \mathbb{R}$ is the bilinear form, $F : V(\mathscr{P}_h) \longrightarrow \mathbb{R}$ the linear 'load' functional, and $\mathscr{P}_h$ denotes the partition of Ω into finite elements (see (3)). In the AVS-FE method, $U(\Omega)$ is a globally continuous Hilbert space as used in mixed and Galerkin FE methods. However, $V(\mathscr{P}_h)$ is a broken space consisting of functions that are globally in $L^2(\Omega)$ and locally may be of higher order (e.g., $H^1(K_m)$). The kernel of $B(\cdot,\cdot)$ is assumed to be trivial to guarantee the uniqueness of solutions (as in any other FE method).

With the assumption on the kernel of the bilinear form in place, the AVS-FE method introduces the following *energy norm* $\|\cdot\|_B : U(\Omega) \longrightarrow [0,\infty)$:

$$\|\mathfrak{u}\|_B \overset{\text{def}}{=} \sup_{\mathfrak{v} \in V(\mathscr{P}_h)\setminus\{\mathbf{0}\}} \frac{|B(\mathfrak{u},\mathfrak{v})|}{\|\mathfrak{v}\|_{V(\mathscr{P}_h)}}. \tag{5}$$

The well posedness of the AVS-FE weak formulation is then established by the following lemma:

Lemma 2.1. *Let the source and Neumann data (if present) be sufficiently regular. Then, the weak formulation (4) is well posed.*

Proof. The proof follows from the Generalized Lax-Milgram Theorem, as $B(\cdot,\cdot)$ satisfies the Inf-sup condition as well as the continuity condition in terms of the energy norm (5), (see [20,26] for details). □

By deriving the weak statement such that the trial space consists of global Hilbert spaces, the AVS-FE method seeks FE approximations $\mathbb{u}^h$ of $\mathbb{u}$ of (4) in which the trial functions in the discretization are FE basis functions that span the FE trial space $U^h(\Omega)$, e.g., $H^1(\Omega)$ or $H(\mathrm{div},\Omega)$. Hence, we represent the approximations of the components $\mathbb{u}^h(\mathbf{x})$ as linear combinations of trial basis functions $e^i(\mathbf{x}) \in U^h(\Omega)$ and the corresponding degrees of freedom, $\mathbb{u}_i^h$. Conversely, to construct the test space $V^*(\mathscr{P}_h)$ we compute piecewise discontinuous *optimal* test functions that guarantee stable discretizations. These optimal test functions are obtained by employing the DPG philosophy [20,24–27] in which *global* optimal test functions are established through *global* weak problems. However, even though the optimal test functions are global functions, they have compact support and, in the case of the AVS-FE method their support is identical to that of the trial functions. Additionally, the local restrictions are computed in a completely decoupled fashion, i.e., element-by-element, with high accuracy (see [19] for details). Thus, e.g., for the local restriction of a trial function $\mathbb{e}^i$ on an element $K_m \in \mathscr{P}_h$, i.e., a shape function, we solve the corresponding optimal test function $\hat{\mathbb{e}}^i(\mathbf{x})$ from the following *local* problem on K_m:

$$\left(\mathbb{r}, \hat{\mathbb{e}}^i\right)_{V(K_m)} = B_{|K_m}(\mathbb{e}^i, \mathbb{r}), \quad \forall \mathbb{r} \in V(K_m), \tag{6}$$

where $B_{|K_m}(\cdot,\cdot)$ denotes the restriction of $B(\cdot,\cdot)$ to the element K_m, $V(K_m)$ the local restriction of the test space to K_m, and $(\cdot,\cdot)_{V(K_m)} : V(K_m) \times V(K_m) \longrightarrow \mathbb{R}$, is a local inner product on $V(K_m)$. see [19] for details. Numerical evidence suggests that the local Riesz representation problems (6) can be solved at the same local order of approximation as the trial function in the RHS of (6). Since this space consists of discontinuous polynomial functions, it is larger than the space of the continuous trial functions, i.e., this is in line with the DPG method of testing with a larger space to attain discrete stability.

Finally, we introduce the FE discretization of (4) governing the approximation $\mathbb{u}^h \in U^h(\Omega)$ of $\mathbb{u}$:

$$\begin{aligned} &\text{Find} \quad \mathbb{u}^h \in U^h(\Omega) \ \text{ such that:} \\ &\qquad B(\mathbb{u}^h, \mathbb{v}^h) = F(\mathbb{v}^h), \quad \forall \mathbb{v}^h \in V^*(\mathscr{P}_h), \end{aligned} \tag{7}$$

where the finite dimensional subspace of test functions $V^*(\mathscr{P}_h) \subset V(\mathscr{P}_h)$ is spanned by the optimal test functions.

By using the DPG philosophy to construct $V^*(\mathscr{P}_h)$, the discrete problem (7) inherits the continuity and inf-sup constants of the continuous problem scaled by the continuity constant of a Fortin type operator [28]. Hence, the AVS-FE discretization is stable for any choice of element size h_m and local degree of polynomial approximation p_m. A further consequence of the optimal test functions is that the global stiffness matrix is symmetric and positive definite regardless of the character of the underlying differential operator.

Remark 2.1. Instead of computing the optimal test functions from (6) on-the-fly to construct the FE system of linear algebraic equations, one can consider another, equivalent, interpretation of the AVS-FE method. This interpretation is in the DPG literature [29–31] referred to as a mixed or saddle point problem and is a result of the fact that DPG and AVS-FE methods are constrained minimization techniques:.

$$\begin{aligned} &\text{Find } \mathbb{u}^h \in U^h(\Omega), \hat{\mathbb{E}}^h \in V^h(\mathscr{P}_h) \ \text{ such that:} \\ &\left(\hat{\mathbb{E}}^h, \mathbb{v}^h\right)_{V(\mathscr{P}_h)} - B(\mathbb{u}^h, \mathbb{v}^h) = -F(\mathbb{v}^h), \quad \forall \mathbb{v}^h \in V^h(\mathscr{P}_h), \\ &\qquad\qquad B(\mathbb{p}^h, \hat{\mathbb{E}}^h) = 0, \quad \forall \mathbb{p}^h \in U^h(\Omega). \end{aligned} \tag{8}$$

The second equation of (8) represents the constraint in which the Gateaux derivative of the bilinear form is acting on the approximate "error representation" function $\hat{\mathbb{E}}^h$. This function is a Riesz representer of the approximation error $\mathbb{u} - \mathbb{u}^h$ and leads to an identity between the energy norm of the approximation error and the norm of the error representation function on $V(\mathscr{P}_h)$. Hence, the norm $\|\hat{\mathbb{E}}\|_{V(\mathscr{P}_h)}$ is an a posteriori error estimate and its local restriction may be employed as an error indicator in mesh adaptive strategies. For details on these error indicators and the derivation of the mixed formulation, see [29] or [32]. Note that since we, at this point, have assumed that the underlying differential operator is linear, the Gateaux derivative of the bilinear form is identical to itself.

This mixed form allows straightforward implementation in high level FE solvers such as Firedrake [33] and FEniCS [34]. The cost of solving the resulting system of linear algebraic equations from (8) is larger than the 'classical' AVS-FE method since now the optimal test functions are essentially computed by solving global problems. However, it has the clear advantage for *hp*-adaptive strategies, since upon solving (8), it immediately provides *a posteriori* error estimators and error indicators that can drive the mesh adaptive process.

3. AVS-FE weak formulation and discretization of the Cahn-Hilliard equation

With the notations introduced in Section 2 and the review of the AVS-FE method above, we proceed to derive the AVS-FE weak formulation for the Cahn-Hilliard IBVP. To this end, let us consider the following general form of the Cahn-Hilliard IBVP (2):

$$\begin{aligned} &\text{Find } u \text{ such that:} \\ &-\frac{\partial u}{\partial t} + D\,\Delta\left[u^3 - u - \lambda\,\Delta\, u\right] = 0, \quad \text{in } \Omega_T, \\ &u = u_0, \quad \text{on } \partial\Omega_T, \\ &u = u_{initial}, \quad \text{on } \Omega, \\ &u^3 - u - \lambda\,\Delta\, u = g, \quad \text{on } \partial\Omega_T, \end{aligned} \tag{9}$$

where $\Omega_T = \Omega \times (0, T)$ is the space-time domain, $\partial\Omega_T$ the space-time boundary excluding the initial and final time surfaces, $D \in L^\infty(\Omega)$, and $\lambda \in L^\infty(\Omega)$. The diffusion coefficient D and the square width of the transition region λ are considered to be constant throughout the domain. To derive the weak formulation, we use a regular partition $\mathscr{P}_T^h$ of Ω_T into elements K_m, such that:

$$\Omega_T = \text{int}\Big(\bigcup_{K_m \in \mathscr{P}_T^h} \overline{K_m}\Big). \tag{10}$$

We apply a mixed FE methodology and introduce two flux variables $\mathbf{r}, \mathbf{t}$ and an additional scalar variable q as auxiliary variables:

- $\mathbf{r} = \{r_x, r_y\}^T = \nabla u$.
- $q = u^3 - u - \lambda\,\nabla \cdot \mathbf{r}$.
- $\mathbf{t} = \{t_x, t_y\}^T = \nabla q$.

Where ∇ denotes the spatial gradient operator. Note that the flux variables vary in time due to the definitions of the scalar variables but are only of dimension Ω. Hence, this dictates that the regularity of these trial functions is $\mathbf{r} \in H(\text{div}, \Omega)$, $\mathbf{t} \in H(\text{div}, \Omega)$, $q \in H^1(\Omega_T)$, $u \in H^1(\Omega_T)$, and the IBVP (9) can be recast as an equivalent first-order system of PDEs:

$$\begin{aligned} &\text{Find } (u, q, \mathbf{r}, \mathbf{t}) \in H^1(\Omega_T) \times H^1(\Omega_T) \times H(\text{div}, \Omega) \times H(\text{div}, \Omega) \text{ such that:} \\ &\nabla u - \mathbf{r} = \mathbf{0}, \quad \text{in } \Omega, \\ &\nabla q - \mathbf{t} = \mathbf{0}, \quad \text{in } \Omega, \\ &u^3 - u - \lambda\,\nabla \cdot \mathbf{r} - q = 0, \quad \text{in } \Omega_T, \\ &-\frac{\partial u}{\partial t} + D\,\nabla \cdot \mathbf{t} = 0, \quad \text{in } \Omega_T, \\ &u = u_0, \quad \text{on } \partial\Omega_T, \\ &u = u_{initial}, \quad \text{on } \Omega, \\ &q = g, \quad \text{on } \partial\Omega_T. \end{aligned} \tag{11}$$

The reason we elect to work with this first-order system structure is to apply the DPG philosophy to construct the optimal test space while using globally continuous FE approximation spaces such as Lagrange and Raviart-Thomas polynomials for the trial space without the need for auxiliary trace unknowns used in the DPG method. We proceed to enforce the PDEs (11) weakly on each element $K_m \in \mathscr{P}_T^h$ and sum the contributions from all $K_m \in \mathscr{P}_T^h$, i.e.,

$$\begin{aligned} &\text{Find } (u, q, \mathbf{r}, \mathbf{t}) \in H^1(\Omega_T) \times H^1(\Omega_T) \times H(\text{div}, \Omega) \times H(\text{div}, \Omega): \\ &\sum_{K_m \in \mathscr{P}_T^h} \int_{K_m} \Big\{ [\nabla u - \mathbf{r}] \cdot \mathbf{s}_m + [\nabla q - \mathbf{t}] \cdot \mathbf{p}_m + \Big[u^3 - u - \lambda\,\nabla \cdot \mathbf{r} - q\Big]\, v_m \\ &\qquad + \Big[-\frac{\partial u}{\partial t} + D\,\nabla \cdot \mathbf{t}\Big]\, w_m \Big\}\, \mathrm{d}\mathbf{x} = 0, \\ &\qquad \forall (v_m, w_m, \mathbf{s}_m, \mathbf{p}_m) \in L^2(\Omega_T) \times L^2(\Omega_T) \times [L^2(\Omega)]^2 \times [L^2(\Omega)]^2. \end{aligned} \tag{12}$$

Next, we apply integration by parts to the terms multiplied with the scalar valued test functions v_m and w_m which dictates that we increase the regularity of each scalar valued test function to be in H^1 locally for every $K_m \in \mathscr{P}_T^h$, i.e.,

$$
\begin{aligned}
&\text{Find } (u, q, \mathbf{r}, \mathbf{t}) \in H^1(\Omega_T) \times H^1(\Omega_T) \times H(\mathrm{div}, \Omega) \times H(\mathrm{div}, \Omega) : \\
&\sum_{K_m \in \mathscr{P}_T^h} \left\{ \int_{K_m} \Big[[\nabla u - \mathbf{r}] \cdot \mathbf{s}_m + [\nabla q - \mathbf{t}] \cdot \mathbf{p}_m + \Big[u^3 - u - q \Big] v_m \right. \\
&\qquad + \lambda\, \mathbf{r} \cdot \nabla v_m - \frac{\partial u}{\partial t}\, w_m - D\, \mathbf{t} \cdot \nabla w_m \Big] \mathrm{d}\mathbf{x} \\
&\qquad \left. + \oint_{\partial K_m} D\, \gamma_{\mathbf{n}}^m(\mathbf{t})\, \gamma_0^m(w_m) - \lambda\, \gamma_{\mathbf{n}}^m(\mathbf{r})\, \gamma_0^m(v_m)\, \mathrm{d}s \right\} = 0, \\
&\qquad\qquad \forall (v_m, w_m, \mathbf{s}_m, \mathbf{p}_m) \in H^1(\mathscr{P}_T^h) \times H^1(\mathscr{P}_T^h) \times [L^2(\Omega)]^2 \times [L^2(\Omega)]^2,
\end{aligned}
\tag{13}
$$

where the broken H^1 space on the partition $\mathscr{P}_T^h$ is defined:

$$
H^1(\mathscr{P}_T^h) \overset{\text{def}}{=} \left\{ v \in L^2(\Omega_T) : \quad v_m \in H^1(K_m),\ \forall K_m \in \mathscr{P}_T^h \right\}. \tag{14}
$$

The operators $\gamma_0^m : H^1(K_m) :\longrightarrow H^{1/2}(\partial K_m)$ and $\gamma_{\mathbf{n}}^m : H(\mathrm{div}, K_m) \longrightarrow H^{-1/2}(\partial K_m)$ denote the trace and normal trace operators (e.g., see [35]) on K_m; and $\mathbf{n}_m$ is the outward unit normal vector to the element boundary ∂K_m of K_m. Note that the edge integrals on ∂K_m are to be interpreted as the duality pairings $\langle \cdot, \cdot \rangle_{H^{-1/2}(\partial K_m) \times H^{1/2}(\partial K_m)}$, instead, we use an integral representation here, as is engineering convention.

Note that the edge integrals in (13) only concern the auxiliary flux unknowns $\mathbf{r}$ and $\mathbf{t}$. Thus, any Dirichlet boundary conditions on u and q must be enforced strongly. Alternatively, we could perform further applications of integration by parts to shift all the derivatives to the test functions, which would allow the weak enforcement of both BCs in (11). Finally, these boundary conditions are incorporated in the space $U(\Omega_T)$ and we arrive at the AVS-FE weak statement for the Cahn-Hilliard IBVP:

$$
\begin{aligned}
&\text{Find } (u, q, \mathbf{r}, \mathbf{t}) \in U(\Omega_T) : \\
&\sum_{K_m \in \mathscr{P}_T^h} \left\{ \int_{K_m} \Big[[\nabla u - \mathbf{r}] \cdot \mathbf{s}_m + [\nabla q - \mathbf{t}] \cdot \mathbf{p}_m + \Big[u^3 - u - q \Big] v_m \right. \\
&\qquad + \lambda\, \mathbf{r} \cdot \nabla v_m - \frac{\partial u}{\partial t}\, w_m - D\, \mathbf{t} \cdot \nabla w_m \Big] \mathrm{d}\mathbf{x} \\
&\qquad \left. + \oint_{\partial K_m} D\, \gamma_{\mathbf{n}}^m(\mathbf{t})\, \gamma_0^m(w_m) - \lambda\, \gamma_{\mathbf{n}}^m(\mathbf{r})\, \gamma_0^m(v_m)\, \mathrm{d}s \right\} = 0, \\
&\qquad\qquad \forall (v_m, w_m, \mathbf{s}_m, \mathbf{p}_m) \in V(\mathscr{P}_T^h),
\end{aligned}
\tag{15}
$$

where the trial and test spaces $U(\Omega_T)$ and $V(\mathscr{P}_T^h)$ are defined:

$$
\begin{aligned}
U(\Omega_T) &\overset{\text{def}}{=} \Big\{ (u, q, \mathbf{r}, \mathbf{t}) \in H^1(\Omega_T) \times H^1(\Omega_T) \times H(\mathrm{div}, \Omega) \times H(\mathrm{div}, \Omega) : \\
&\quad \gamma_0^m(u)_{|\partial K_m \cap \partial \Omega_T} = u_0, \gamma_0^m(q)_{|\partial K_m \cap \partial \Omega_T} = g,\ \forall K_m \in \mathscr{P}_T^h \Big\}, \\
V(\mathscr{P}_T^h) &\overset{\text{def}}{=} H^1(\mathscr{P}_T^h) \times H^1(\mathscr{P}_T^h) \times [L^2(\Omega)]^2 \times [L^2(\Omega)]^2,
\end{aligned}
\tag{16}
$$

with norms $\|\cdot\|_{U(\Omega_T)} : U(\Omega_T) \longrightarrow [0, \infty)$ and $\|\cdot\|_{V(\mathscr{P}_T^h)} : V(\mathscr{P}_T^h) \longrightarrow [0, \infty)$ defined as:

$$
\begin{aligned}
\|(u, q, \mathbf{r}, \mathbf{t})\|_{U(\Omega_T)} &\overset{\text{def}}{=} \sqrt{\int_{\Omega_T} \Big[(u, u)_{H^1(\Omega_T)} + (q, q)_{H^1(\Omega_T)} + (\mathbf{r}, \mathbf{r})_{H(\mathrm{div}, \Omega)} + (\mathbf{t}, \mathbf{t})_{H(\mathrm{div}, \Omega)} \Big] \mathrm{d}\mathbf{x}}, \\
\|(v, w, \mathbf{s}, \mathbf{p})\|_{V(\mathscr{P}_T^h)} &\overset{\text{def}}{=} \\
&\sqrt{\sum_{K_m \in \mathscr{P}_T^h} \int_{K_m} \Big[h_m^2 \nabla v_m \cdot \nabla v_m + v_m^2 + h_m^2 \nabla w_m \cdot \nabla w_m + w_m^2 + \mathbf{s}_m \cdot \mathbf{s}_m + \mathbf{p}_m \cdot \mathbf{p}_m \Big] \mathrm{d}\mathbf{x}}.
\end{aligned}
\tag{17}
$$

Note that the scaled norm $\|\cdot\|_{V(\mathscr{P}_T^h)}$ is equivalent to the L^2 norm on $V(\mathscr{P}_T^h)$ (with mesh-dependent equivalence constants):

$$\|(v, w, \mathbf{s}, \mathbf{p})\|_V \overset{\text{def}}{=} \sqrt{\sum_{K_m \in \mathscr{P}_T^h} \int_{K_m} \left[v_m^2 + w_m^2 + \mathbf{s}_m \cdot \mathbf{s}_m + \mathbf{p}_m \cdot \mathbf{p}_m \right] \mathrm{d}\mathbf{x}}. \tag{18}$$

Our choice for the test space norm $\|\cdot\|_{V(\mathscr{P}_T^h)}$ is motivated by the wish to keep all terms in the integral that defines the norm of similar magnitude. This in turn leads to a stiffness matrix in which the entries are of similar magnitude which is beneficial for the conditioning of the linear system of equations. By introducing the operator $B : U(\Omega_T) \times V(\mathscr{P}_T^h) \longrightarrow \mathbb{R}$:

$$\begin{aligned} B((u, q, \mathbf{r}, \mathbf{t}); (v, w, \mathbf{s}, \mathbf{p})) \overset{\text{def}}{=} \sum_{K_m \in \mathscr{P}_T^h} \Bigg\{ \int_{K_m} \Big[& [\nabla u - \mathbf{r}] \cdot \mathbf{s}_m + [\nabla q - \mathbf{t}] \cdot \mathbf{p}_m + \left[u^3 - u - q \right] v_m \\ & + \lambda\, \mathbf{r} \cdot \nabla v_m - \frac{\partial u}{\partial t}\, w_m - D\, \mathbf{t} \cdot \nabla w_m \Big] \mathrm{d}\mathbf{x} \\ & + \oint_{\partial K_m} D\, \gamma_{\mathbf{n}}^m(\mathbf{t})\, \gamma_0^m(w_m) - \lambda\, \gamma_{\mathbf{n}}^m(\mathbf{r})\, \gamma_0^m(v_m)\, \mathrm{d}s \Bigg\}, \end{aligned} \tag{19}$$

we can write the weak formulation (15) compactly:

$$\boxed{\begin{aligned} &\text{Find } (u, q, \mathbf{r}, \mathbf{t}) \in U(\Omega_T) \text{ such that:} \\ &\quad B((u, q, \mathbf{r}, \mathbf{t}); (v, w, \mathbf{s}, \mathbf{p})) = 0, \quad \forall (v, w, \mathbf{s}, \mathbf{p}) \in V(\mathscr{P}_T^h). \end{aligned}} \tag{20}$$

See Appendix A for a well-posedness analysis of an AVS-FE weak formulation (20) for a linearized Cahn-Hilliard BVP.

3.1. AVS-FE discretizations

We seek numerical approximations $(u^h, q^h, \mathbf{r}^h, \mathbf{t}^h)$ of $(u, q, \mathbf{r}, \mathbf{t})$ by using FE trial basis functions such as Lagrange interpolants or Raviart-Thomas polynomials. However, the test space is discretized by employing the DPG philosophy and we use optimal test functions as computed from the discrete Riesz problems (see (4)). Thus, the FE discretization of (20) governing $(u^h, q^h, \mathbf{r}^h, \mathbf{t}^h) \in U^h(\Omega_T)$ is:

$$\boxed{\begin{aligned} &\text{Find } (u^h, q^h, \mathbf{r}^h, \mathbf{t}^h) \in U^h(\Omega_T) \text{ such that:} \\ &\quad B((u^h, q^h, \mathbf{r}^h, \mathbf{t}^h); (v^h, w^h, \mathbf{s}^h, \mathbf{p}^h)) = 0, \quad \forall (v^h, w^h, \mathbf{s}^h, \mathbf{p}^h) \in V^*(\mathscr{P}_T^h), \end{aligned}} \tag{21}$$

where the finite dimensional test space $V^*(\mathscr{P}_T^h) \subset V(\mathscr{P}_T^h)$ is spanned by numerical approximations of the test functions through the Riesz representation problems, analogous to (6).

By exploiting the discrete stability of the AVS-FE method, the entire space-time domain is discretized by finite elements instead of using traditional time stepping techniques satisfying a CFL condition. Hence, we have significant flexibility in the choice of mesh parameters in the FE discretization.

To solve the nonlinear variational problem, we can linearize the weak form and solve a sequence of linear discrete problems that converge to the nonlinear solution. This can be achieved by employing solution procedures such as Newton iterations to (21) to which we compute on-the-fly optimal test functions at each step of the Newton iterations. However, we consider an equivalent mixed or saddle point problem interpretation of the AVS-FE method, as introduced in Section 2.2, in which we seek both $(u^h, q^h, \mathbf{r}^h, \mathbf{t}^h)$ and the error representation function $(\psi^h, \varphi^h, \boldsymbol{\xi}^h, \boldsymbol{\eta}^h)$:

$$\boxed{\begin{aligned} &\text{Find } (u^h, q^h, \mathbf{r}^h, \mathbf{t}^h) \in U^h(\Omega_T), (\psi^h, \varphi^h, \boldsymbol{\xi}^h, \boldsymbol{\eta}^h) \in V^h(\mathscr{P}_T^h) \text{ such that:} \\ &\Big((\psi^h, \varphi^h, \boldsymbol{\xi}^h, \boldsymbol{\eta}^h), (v^h, w^h, \mathbf{s}^h, \mathbf{p}^h) \Big)_{V(\mathscr{P}_T^h)} - B((u^h, q^h, \mathbf{r}^h, \mathbf{t}^h); (v^h, w^h, \mathbf{s}^h, \mathbf{p}^h)) = 0, \\ &\qquad \forall (v^h, w^h, \mathbf{s}^h, \mathbf{p}^h) \in V^h(\mathscr{P}_T^h), \\ &B'_{\mathfrak{u}}((a^h, b^h, \mathbf{c}^h, \mathbf{d}^h); (\psi^h, \varphi^h, \boldsymbol{\xi}^h, \boldsymbol{\eta}^h)) = 0, \\ &\qquad \forall\, ((a^h, b^h, \mathbf{c}^h, \mathbf{d}^h)) \in U^h(\Omega_T). \end{aligned}} \tag{22}$$

Where the operator $B'_{\mathfrak{u}} : U(\Omega_T) \times V(\mathscr{P}_T^h) \longrightarrow \mathbb{R}$ is the first order Gateaux derivative of the sesquilinear form B with respect to $\mathfrak{u} = (u, q, \mathbf{r}, \mathbf{t})$. Application of the definition of the Gateaux derivative then gives:

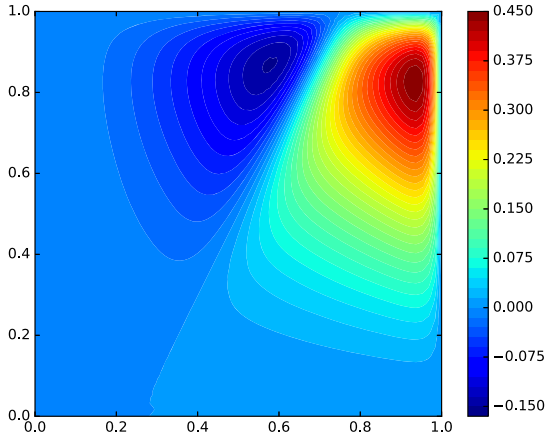

Fig. 2. Exact solution $u(x, y)$ of the propagating front problem. (For interpretation of the colors in the figure(s), the reader is referred to the web version of this article.)

$$
\begin{aligned}
B'_{\mathbb{u}1}((a,b,\mathbf{c},\mathbf{d});(\psi,\varphi,\boldsymbol{\xi},\boldsymbol{\eta})) \overset{\text{def}}{=} \sum_{K_m\in\mathscr{P}_T^h}\Bigg\{\int_{K_m}\Big[&[\nabla a-\mathbf{c}]\cdot\boldsymbol{\xi}_m+[\nabla b-\mathbf{d}]\cdot\boldsymbol{\eta}_m\\
&+\left[3u^2a-a-b\right]\psi_m+\beta\,\mathbf{c}\cdot\nabla\psi_m-\frac{\partial a}{\partial t}\varphi_m-D\,\mathbf{d}\cdot\nabla\varphi_m\Big]\,\mathrm{d}\mathbf{x}\\
&+\oint_{\partial K_m} D\,\gamma_{\mathbf{n}}^m(\mathbf{d})\,\gamma_0^m(\varphi_m)-\beta\,\gamma_{\mathbf{n}}^m(\mathbf{c})\,\gamma_0^m(\psi_m)\,\mathrm{d}s\Bigg\}
\end{aligned}
\tag{23}
$$

4. Numerical verifications

In this section, we present several numerical verifications applying the AVS-FE method to stationary and transient problems. To establish the solution of (22) we use the high-level FE solvers Firedrake [33] and FEniCS [34] which in turn employ the Portable, Extensible Toolkit for Scientific Computation (PETSc) library Scalable Nonlinear Equations Solvers (SNES) [36,37] to perform Newton iterations. In all experiments presented, we use PETSc SNES objects in Firedrake [33] and FEniCS [34] with the default settings for tolerances for the iterations.

4.1. Numerical convergence studies

To ascertain the convergence behavior of the AVS-FE method for the Cahn-Hilliard equation, we perform multiple verifications of its convergence properties. We first consider a stationary model problem where we consider a manufactured exact solution $u(x, y)$ slightly modified from [38] called the *propagating front test case*:

$$
u(x,y)=(x\,y)\tanh\left(\frac{x-0.5y-0.25}{\sqrt{2\lambda}}\right)\left(x+\frac{e^{50x}-1}{1-e^{50}}\right)\left(y+\frac{e^{10x}-1}{1-e^{10}}\right). \tag{24}
$$

To impose this exact solution, we apply the Cahn-Hilliard equation (2) to (24) to ascertain a corresponding nonzero right hand side and Dirichlet boundary conditions on u and q, we pick $D=1$, $\lambda=1/320$, and the domain as the unit square i.e., $\Omega=(0,1)\times(0,1)$. This exact solution is shown in Fig. 2. The function spaces we use for this verification consist of Raviart-Thomas and Lagrangian bases for the $H(\mathrm{div},\Omega)$ and $H^1(\Omega)$ approximations, respectively as well as their discontinuous counterparts for $H(\mathrm{div},\mathscr{P}_h)$ and $H^1(\mathscr{P}_h)$. In the mixed problem we solve (22), we pick basis functions for the solution $(u^h,q^h,\mathbf{r}^h,\mathbf{t}^h)$ and the error representation function $(\psi^h,\varphi^h,\boldsymbol{\xi}^h,\boldsymbol{\eta}^h)$ of identical approximation order.

We implement the two-dimensional problem in FEniCS and start with a uniform mesh consisting of two triangular elements to which we perform both uniform and adaptive h-refinements. For uniform mesh refinements, we establish the corresponding rates of convergence to ensure optimal behavior. For the base variable u, the expected rates of convergence in Sobolev type norms for a linear fourth order PDE are:

$$
\begin{aligned}
\|u-u^h\|_{L^2(\Omega)} &\leq C\,h^p \quad \text{if } p<3,\\
\|u-u^h\|_{L^2(\Omega)} &\leq C\,h^{p+1} \quad \text{if } p\geq 3,\\
\|u-u^h\|_{H^1(\Omega)} &\leq C\,h^p.
\end{aligned}
\tag{25}
$$

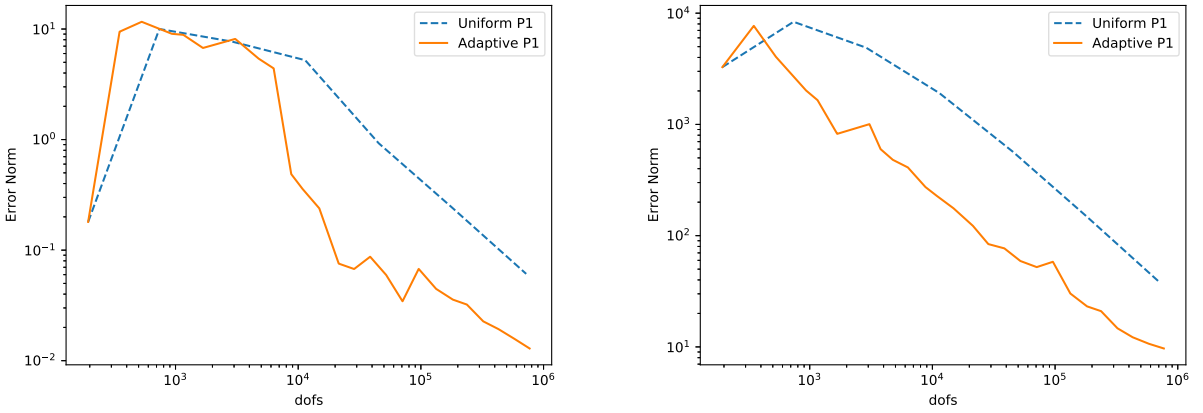

(a) $\|u-u^h\|_{L^2(\Omega)}$. (b) $\|q-q^h\|_{L^2(\Omega)}$.

Fig. 3. Convergence of uniform and adaptive refinements for the stationary case, linear approximations.

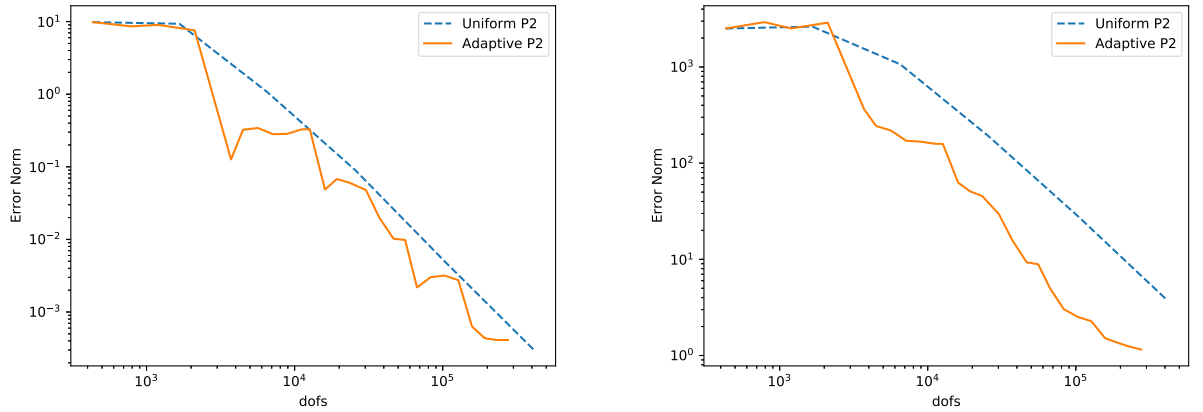

(a) $\|u-u^h\|_{L^2(\Omega)}$. (b) $\|q-q^h\|_{L^2(\Omega)}$.

Fig. 4. Convergence of uniform and adaptive refinements for the stationary case, quadratic approximations.

See [39] and references therein for error estimates of the Cahn-Hilliard equation and fourth order PDEs. Note that for $p<3$, the L^2 and H^1 norms of the approximation error converge at the same rate since the estimates depend upon the order of the PDE $2m=4$.

Due to the implementation of the AVS-FE method as a mixed problem (22), we establish both the approximate solutions $u^h, q^h, \mathbf{r}^h, \mathbf{t}^h$ and the error representation function $(\psi^h, \varphi^h, \boldsymbol{\xi}^h, \boldsymbol{\eta}^h)$. Hence, for the h-adaptive algorithm, we use the restriction of this estimate to each element as an error indicator:

$$\eta = \|(\psi^h, \varphi^h, \boldsymbol{\xi}^h, \boldsymbol{\eta}^h)\|_{V(K_m)} \tag{26}$$

This error indicator has been successfully applied for the AVS-FE method for the linear convection-diffusion PDE and to several classes of problems of the DPG [24,27]. In particular, in [24], (see Theorem 2.1) Carstensen et al. investigate and verify the robustness of this error estimate and corresponding indicators under the requirement of existence of a Fortin operator [28,40]. Without such a Fortin operator, discrete stability and convergence of DPG and AVS-FE methods would not be possible. To mark elements for refinement, we consider the strategy of Dörfler [41], based on the approximate total energy error. The stabilized adaptive method of Calo et al. introduced in [21] also utilizes this type refinement strategy and error indicator.

In Figs. 3, 4, and 5 we present the convergence histories for both adaptive and uniform mesh refinements for increasing orders of approximation. The observed uniform convergence rates in $\|u-u^h\|_{L^2(\Omega)}$ for the uniform refinements are $h^{p+0.9}, h^{p+2}$ and h^{p+1}, for linear, quadratic and cubic approximations, respectively. For the linear and quadratic case these rates are higher than expected in (25), whereas the convergence rates in the H^1 norm are identical to those in (25). The observed uniform convergence rates in the L^2 error $\|q-q^h\|_{L^2(\Omega)}$ for the uniform refinements are h^p, h^{p+1} and $h^{p+0.7}$, for

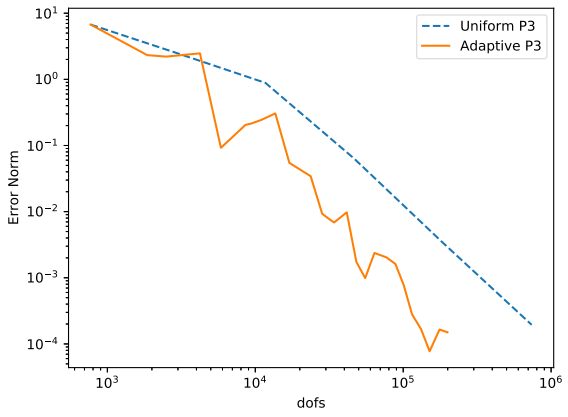

(a) $\|u - u^h\|_{L^2(\Omega)}$.

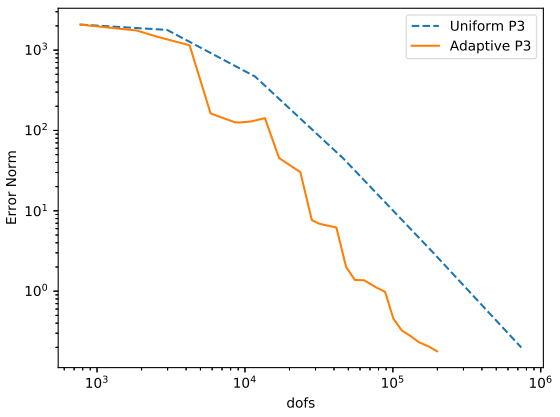

(b) $\|q - q^h\|_{L^2(\Omega)}$.

Fig. 5. Convergence of uniform and adaptive refinements for the stationary case, cubic approximations.

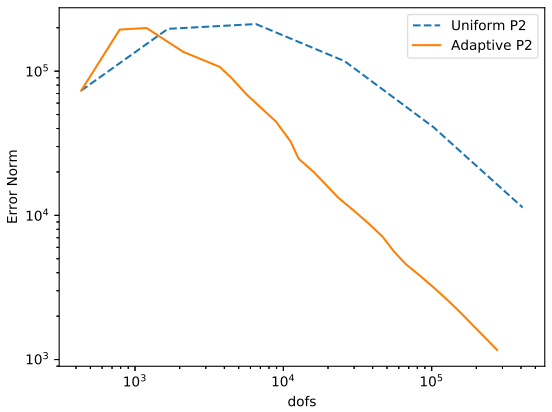

(a) $\|(u, q, \mathbf{r}, \mathbf{t}) - (u^h, q^h, \mathbf{r}^h, \mathbf{t}^h)\|_B$.

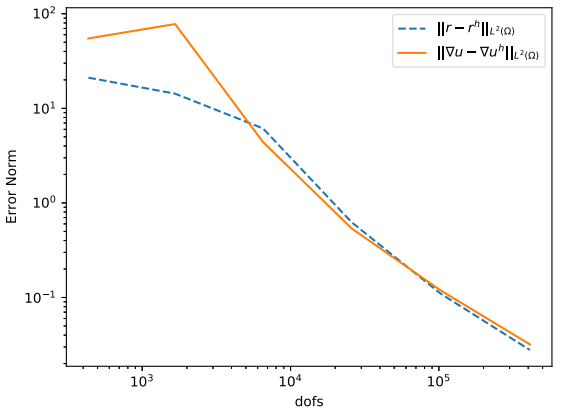

(b) Gradient and flux approximation comparison.

Fig. 6. Convergence results for the stationary Cahn-Hilliard problem.

linear, quadratic and cubic approximations, respectively. In all cases, the adaptive refinements lead to lower errors than the uniform refinements as expected as shown in Figs. 3, 4, and 5.

While the adaptive refinement strategy delivers lower errors than uniform refinements in terms of the L^2 errors of the base variable u, the difference between uniform and adaptive refinements is significantly more noticeable in terms of the energy norm as shown in Fig. 6(a). The difference between the two curves is about an order of magnitude. The reason for this large disparity between the two refinement procedures is our choice of error indicator, which is a local representation of the energy norm, as well as the refinement criterion based on the total energy error. Hence, in the adaptive strategy, the goal is to minimize the energy error. In Fig. 6(b) we compare the L^2 errors of ∇u and the vector variable $\mathbf{r}$ for the case of quadratic approximations under uniform refinement. The difference between the two is marginal in this case with the vector variable being slightly more accurate for the finest mesh.

To present a sequence of adaptively refined meshes, we consider the case of first order approximations. In Figs. 7, 8, and 9 we show selected meshes and corresponding solutions from the refinement process. The built-in error indicator performs very well as the mesh refinements are focused along the propagating front.

Next, we consider a transient model problem to verify the convergence behavior of the space-time AVS-FE method. To this end, we consider the exact solution:

$$u(x, y, t) = \sin(\pi t)\sin(\pi y)\sin(\pi x), \tag{27}$$

and consider the space-time domain $\Omega_T = (0, 1) \times (0, 1) \times (0, 0.1)$. This exact solution is used to ascertain a nonzero source term by applying the Cahn-Hilliard differential operator as well as initial and Dirichlet boundary conditions. The parameters D and λ are both chosen to be unity for simplicity. In the same fashion as the stationary example, we compare both uniform and adaptive mesh refinements based on the same principles. We discretize all continuous variables using equal

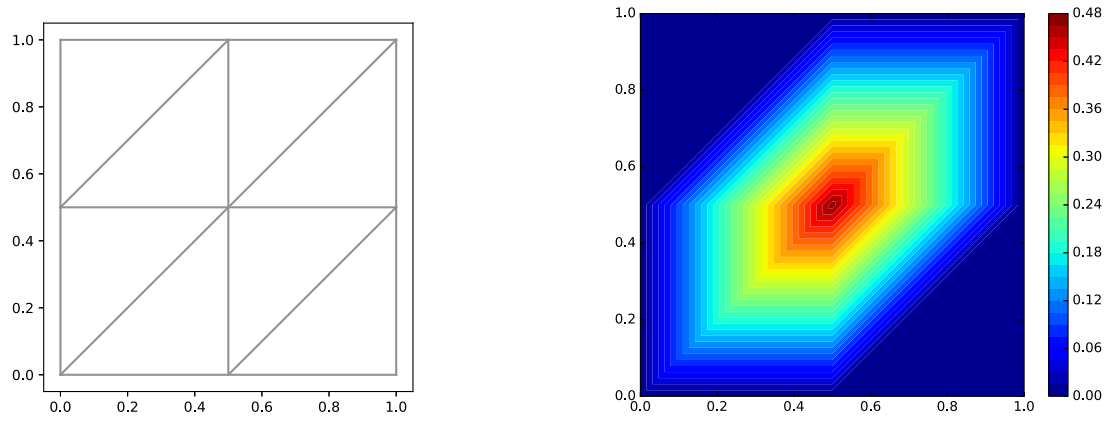

(a) Mesh. (b) Solution u^h.

Fig. 7. Initial adaptive step.

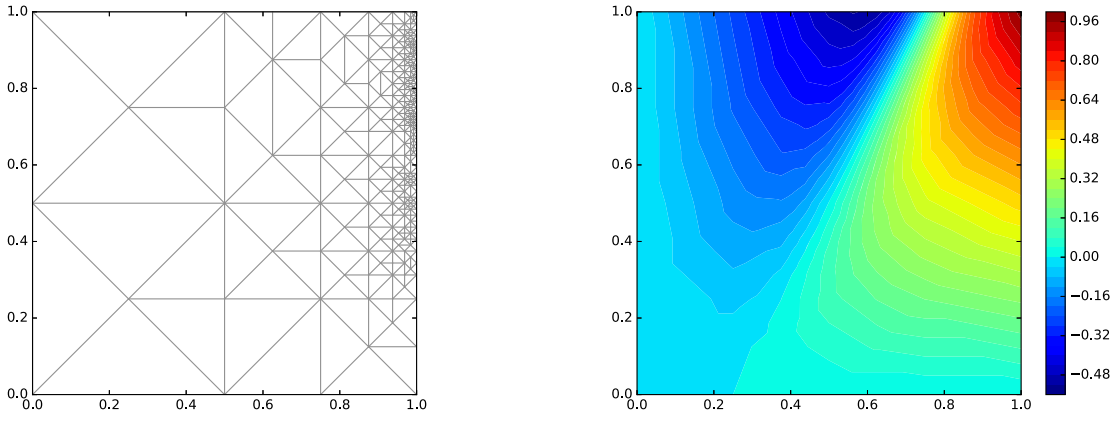

(a) Mesh. (b) Solution u^h.

Fig. 8. 10'th adaptive step.

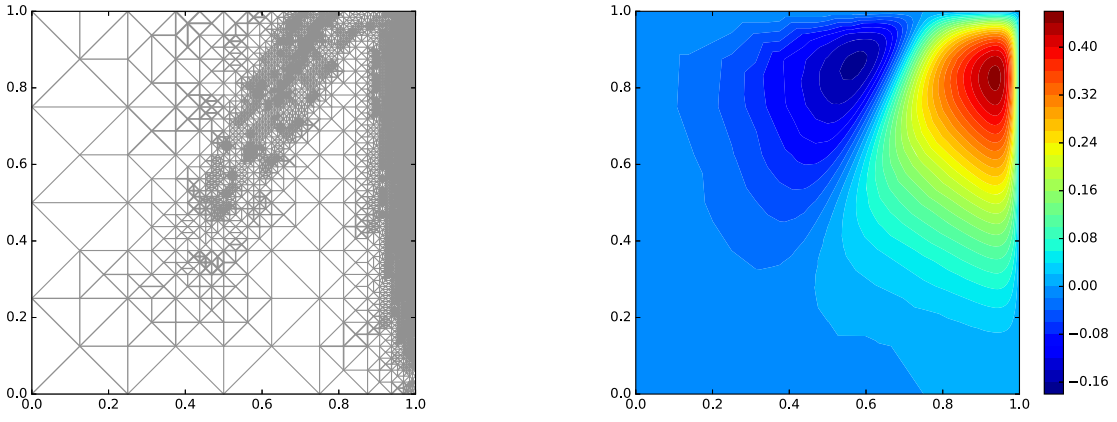

(a) Mesh. (b) Solution u^h.

Fig. 9. 25'th adaptive step.

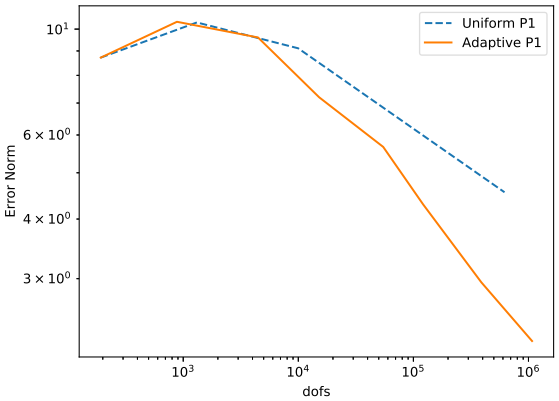

(a) $\|(u,q,\mathbf{r},\mathbf{t}) - (u^h,q^h,\mathbf{r}^h,\mathbf{t}^h)\|_{U(\Omega_T)}$.

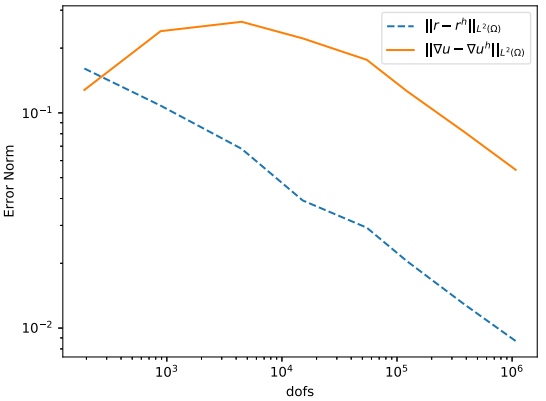

(b) Gradient and flux approximation comparison for adaptive refinements.

Fig. 10. Convergence results for the transient Cahn-Hilliard problem for linear basis functions.

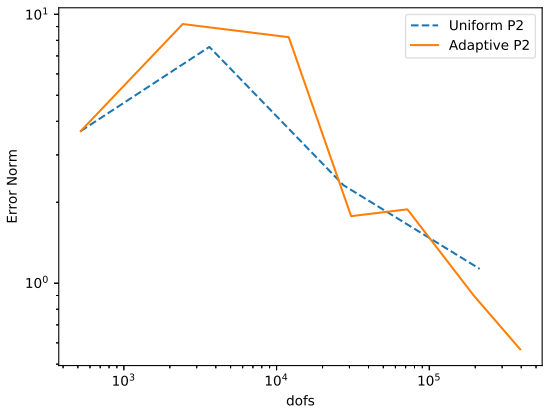

(a) $\|(u,q,\mathbf{r},\mathbf{t}) - (u^h,q^h,\mathbf{r}^h,\mathbf{t}^h)\|_{U(\Omega_T)}$.

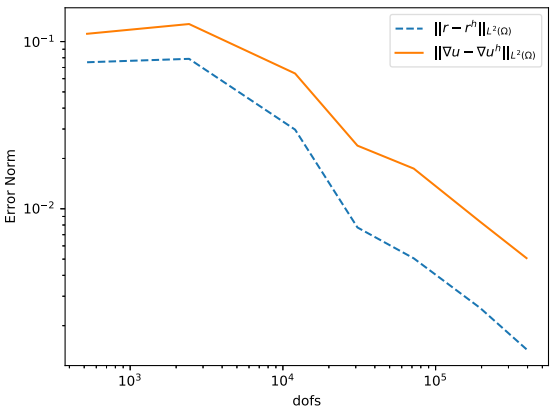

(b) Gradient and flux approximation comparison for adaptive refinements.

Fig. 11. Convergence results for the transient Cahn-Hilliard problem for quadratic basis functions.

order Lagrange polynomial functions in this case to show its effect on the accuracy of the flux variables as compared to the Raviart-Thomas approximations in the previous case. Since the source resulting from the transient exact solution (27) is smooth, the resulting regularity of the flux variables $\mathbf{r}, \mathbf{t}$ is higher than $H(div)$. Hence, the increased regularity of the approximation will not lead to consistency issues. All components of the error representation function are discretized using discontinuous Lagrange polynomials of the same order as the continuous trial variables. In Figs. 10(a) and 11(a) the convergence histories in terms of the total norm on $U(\Omega_T)$ for linear and quadratic approximations are shown. The rates of convergence of the uniform refinements are h^p and $h^{p-0.1}$, for linear and quadratic approximations, respectively. Since this norm contains the H^1 norm of u, we expect h^p convergence, as indicated in (25). The preasymptotic range of convergence ends at roughly 60,000 and 80,000 degrees of freedom for linear and quadratic approximations, respectively, at which point the adaptive refinements become superior. In the quadratic case, the difference between uniform and adaptive refinements is less pronounced in this preasymptotic range as the second order polynomials better approximate the sinusoidal exact solution. In Figs. 10(b) and 11(b) we compare the errors in the flux variable $\mathbf{r}$ and the gradient ∇u for the case of adaptive mesh refinements. For both degrees of approximation we consider, the error in the flux variable is significantly lower than in the gradient. Compared to the stationary case in Fig. 6(b), the effect is more pronounced for the transient problem. We attribute this to the convective nature of the time derivative term which has the greatest benefits of the stability property of the AVS-FE approximations.

4.2. Phase transition problem

In this section we consider a two-dimensional benchmark problem for the Cahn-Hilliard equation as the target physical application of mineral separation falls into this category. This commonly applied problem for the Cahn-Hilliard equation

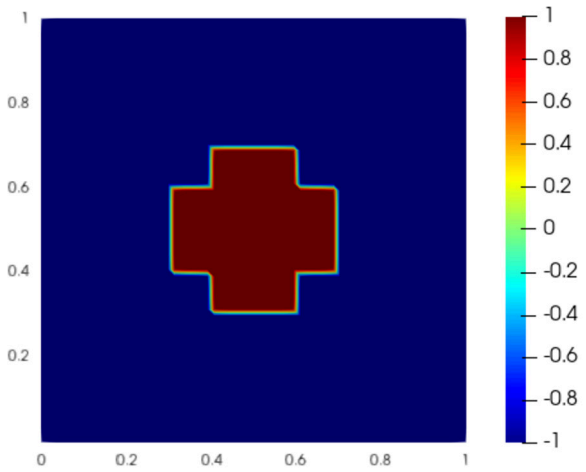

Fig. 12. Initial condition for the two-dimensional model problem.

(a) $t = 0.0015625s$. (b) $t = 0.0046875s$.

Fig. 13. AVS-FE approximation u^h of Cahn-Hilliard equation with initial condition shown in Fig. 12.

governs the evolution of two distinct phases in a medium, see, e.g., [42,43]. The problem is chosen as it depicts a phase transformation and convergence towards a steady state. We consider physical properties as chosen by Brenner et al. [43]: $D = 1$, $\lambda = 0.01$, and the spatial domain consist of the unit square. The domain is initially occupied by two phases of material, one of which is shaped like a cross. Inside the cross, the phase is given the value $+1$ whereas it is -1 outside the cross. This initial condition is given by the piecewise constant function shown in Fig. 12. Based on this initial condition, the boundary conditions are $u = -1$ and $q = 0$ on $\partial\Omega$.

To facilitate visual comparison with the results presented by Brenner et al. [43], we consider a case in which the final time $T = 0.015625$ s, as the binary mixture is expected to have reached a steady state at this time. The computations are performed on a fixed uniform mesh by employing the "extruded mesh" feature of Firedrake [33]. To this end, we consider the case in which Ω_T is discretized by 64×64 triangular elements spatially that are extruded into triangular prism elements in the time domain of width equal to half the final time. We use linear polynomials spatially and fifth order polynomials in time for all continuous and discontinuous trial variables in this case. Other choices of mesh partitions and approximation orders are possible as the method remains stable for any choice of h and p. However, this choice is based upon extensive numerical experimentation as it provides good accuracy for a coarse mesh partition in time consisting of only two elements. In Figs. 13 and 14, the solution is shown at $t = 0.0015625$ s, 0.0046875 s, 0.09375 s and 0.015625 s, respectively. The transformation of the binary phases from the initial to the steady state proceeds as expected and at the final time has reached the steady state in which the two phases are separated by a circle.

Using the AVS-FE method in both space and time makes the comparison to other FE methods for the Cahn-Hilliard equation using the method of lines non-trivial and inappropriate since the computational cost is distributed in a completely different fashion. In terms of accuracy, the AVS-FE method delivers comparable results to those reported in, e.g., [42,43] based on visual inspection and comparison of the results. The consideration of computational complexity is postponed to future research efforts in which other methods are to be considered for the time discretization. For this particular problem, the total number of degrees of freedom is $2,094,797$, while the number of degrees of freedom corresponding to the solution variables $(u^h, q^h, \mathbf{r}^h, \mathbf{t}^h)$ is $371,800$.

(a) $t = 0.09375s$. (b) $t = 0.015625s$.

Fig. 14. AVS-FE approximation u^h of Cahn-Hilliard equation with initial condition shown in Fig. 12.

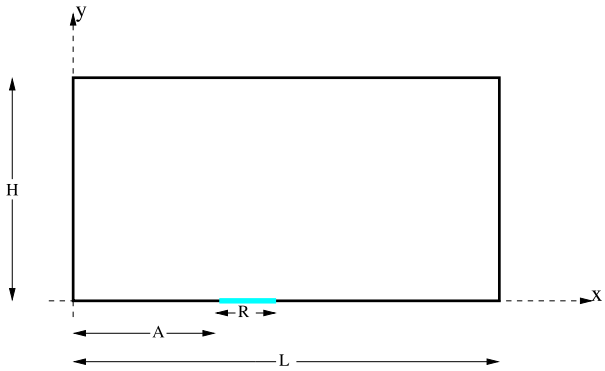

Fig. 15. 2D mineral separation model domain.

4.3. Mineral separation

The development of the space-time AVS-FE method for the Cahn-Hililiard equation was to model the mineral separation process described in Section 1. Thus, here we consider the application of the Cahn-Hilliard equation for the analysis of a mineral separation experiment. The experimental setup consists of a closed box into which a mineral powder is introduced and the separation process takes place on a substrate (see blue section in Fig. 15) which has been treated to attract the desirable mineral particles. The accumulated mineral on the substrate disk is then collected in an appropriate fashion and for the sake of simplicity, we consider only the mineral accumulation in this model. The computational domain is a cross section of the experimental separator and is rectangular with part of its boundary being the treated disk, as shown in Fig. 15. The physical dimensions shown in this figure are: $H = 0.3048$ m, $L = 0.6604$ m, $A = 0.254$ m, and $R = 0.1397$ m, i.e. $\Omega = (0, 0.6604\text{ m}) \times (0, 0.3048\text{ m})$. Particularly, the region R in Fig. 15 represents the substrate and is the location of the mineral accumulation.

In this heuristic model we pick parameters $D = 1$ and $\lambda = 0.1$. Note that the proper physical parameters are to be estimated using an inverse finite element process using experimental data from the experiment in the ongoing design process. The initial condition is a concentration of 0 throughout the domain Ω and to model the buildup of minerals, we employ a Dirichlet boundary condition with a mineral concentration equal to 1 over the disk region. The remainder of the boundary $\partial\Omega$ is considered to have zero mineral concentration. We implement this problem in the same fashion as the preceding verification in Firedrake [33] and use a fixed uniform mesh. Hence, the mesh partition consists of 64×64 triangular elements extruded into two space-time triangular prisms and the basis functions are polynomials that are linear in space and fourth order in time.

In Figs. 16, 17, and 18 the buildup of mineral is shown at times $t = 0.001$ s, 0.002 s, and 0.004 s respectively. As expected, the mineral layer grows vertically since we do not incorporate effects of airflow in this case. Hence, we conclude that the Cahn-Hilliard equation is an appropriate model for the buildup of material in the proposed mineral processing application.

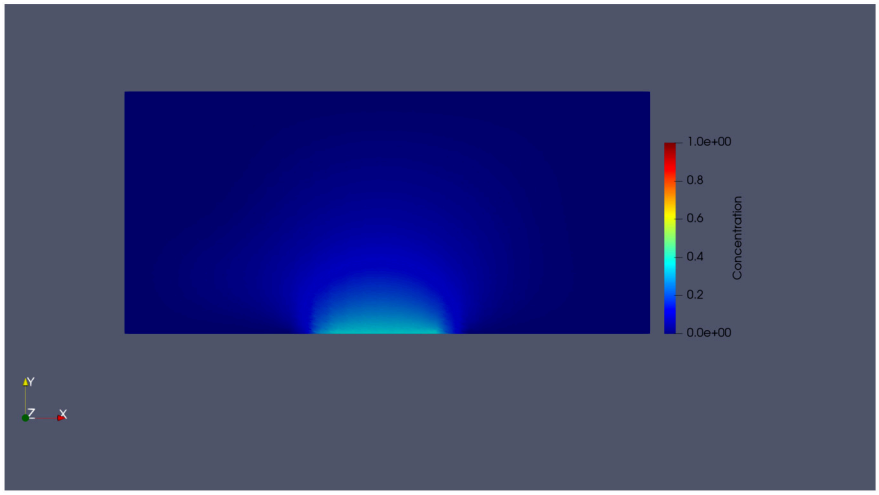

Fig. 16. Mineral separation process at $t = 0.001$ s.

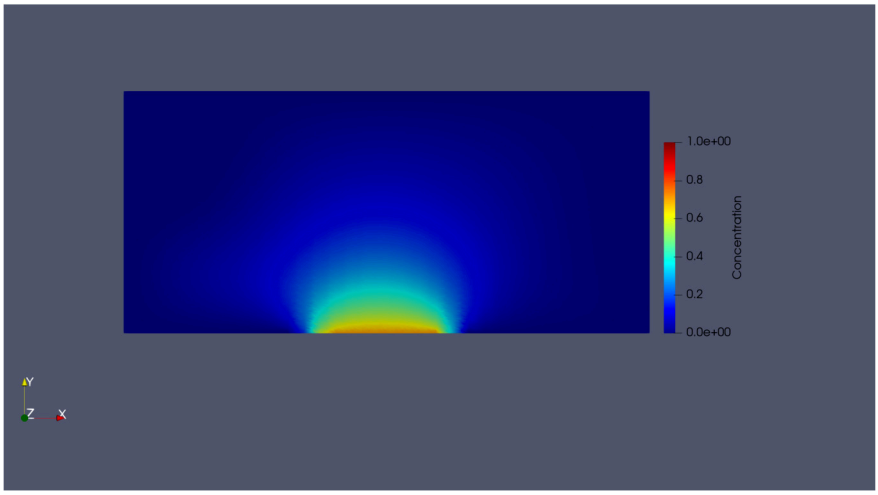

Fig. 17. Mineral separation process at $t = 0.002$ s.

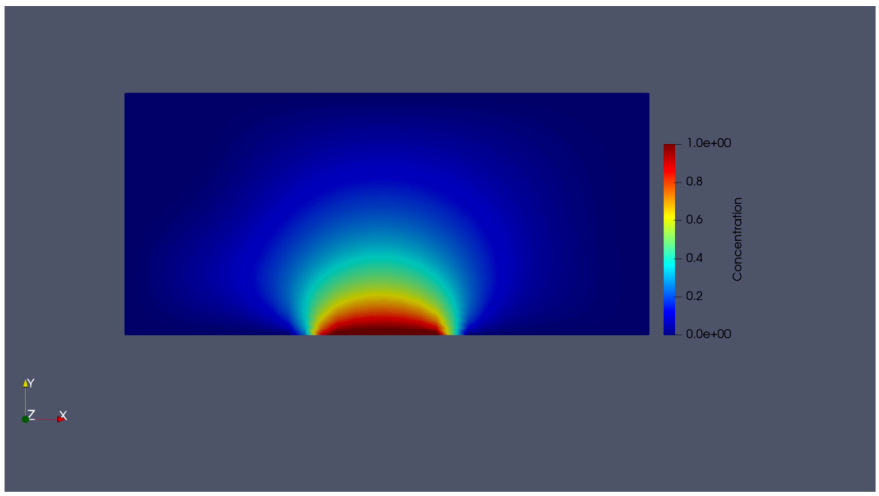

Fig. 18. Mineral separation process at $t = 0.004$ s.

5. Conclusions

We have presented an application of the AVS-FE method to the Cahn-Hilliard equation to establish stable AVS-FE approximations of the Cahn-Hilliard equation in both space and time.

The AVS-FE method results in FE approximations that converge to the exact solution at optimal rates. This was illustrated by both stationary and transient two-dimensional verifications to which manufactured solutions exist in Section 4.1. Furthermore, the AVS-FE method comes with a built-in error estimate and the resulting error indicator has been used to successfully drive mesh adaptive refinements in both space and time. As expected, the adaptive mesh refinements deliver lower FE approximation errors in appropriate norms than uniform refinements. A benchmark problem from literature was also implemented in which the Cahn-Hilliard problem leads to a phase transition between two binary phases in a medium. The results for this case show that the AVS-FE method is capable of delivering accurate space-time computations for spatially two-dimensional problems requiring only a single nonlinear global solve. Finally, in an effort to verify and Cahn-Hilliard equations as a model for the mineral separation application of interest we consider a heuristic model problem governing the growth of a mineral in a simplified mineral separator.

Focus is given here to the use of the AVS-FE method in both space and time due to its discrete stability. Other time discretizations can also be considered, e.g., finite difference techniques or generalized α method [44,45]. For now we leave these techniques for future works that involve spatially three-dimensional problems, in which the space time approach of this paper becomes less feasible due to the need for four-dimensional mesh generation. While the computational cost of the space-time AVS-FE approach we have presented in this paper is high compared to existing techniques it has the advantage that we it solves transient BVPs using a single global solve in space and time. Additionally, the stability property of the AVS-FE enables users to start with a very coarse space-time mesh which can be adaptively refined using the built-in error indicator. Hence, our method is a viable option to existing time stepping algorithms, and the entire solution process is easily amendable to parallel processing. Furthermore, a static condensation process through a Schur complement can further reduce the computational cost. While we have not implemented this in our current computational framework it is to be one of our foci for future research efforts as well as implementation into other DPG FE software such as Camellia [46]. The existence of a Fortin operator [28,40] is at this point based on conjecture from numerical experiments and future research will attempt a mathematical construction of these operators for the AVS-FE method. Currently, the development of an inverse FE process to estimate the physical parameters D and λ for the mineral separation application is ongoing.

CRediT authorship contribution statement

Eirik Valseth: Conceptualization, Formal analysis, Methodology, Software, Supervision, Writing – original draft, Writing – review & editing. **Albert Romkes:** Funding acquisition, Project administration, Supervision, Writing – review & editing. **Austin R. Kaul:** Software, Writing – review & editing.

Declaration of competing interest

The authors declare that they have no known competing financial interests or personal relationships that could have appeared to influence the work reported in this paper.

Acknowledgements

The authors are grateful for the contributions of Professor Jon Kellar, Professor William Cross, and Mr. Bernardo Sansao of the Department of Materials and Metallurgical Engineering at the SDSM&T through fruitful discussions on mineral separation and the Cahn-Hilliard equation.

This work has been supported by the National Science Foundation (NSF) CBET Program, under NSF Grant Number 1805550.

Appendix A

To establish the well-posedness of the AVS-FE weak formulation (20) we apply the Babuška Lax-Milgram Theorem [47]. To accomplish this, we follow the steps of Carstensen, Demkowicz and Gopalakrishnan [48] to show that the stability of the AVS-FE weak formulation is inherited from its unbroken counterpart. Hence, we proceed by first showing the well-posedness of a mixed weak form of a linear Cahn-Hilliard problem, and subsequently showing that the corresponding weak form with a broken test space is well posed as a consequence. In the following, we denote by C a generic mesh independent constant.

For this analysis, we consider a simplified linear and stationary form of the Cahn-Hilliard BVP:

Find u such that:

$$\begin{aligned} D\,\Delta\,[-u - \lambda\,\Delta\,u] &= f, \quad \text{in } \Omega, \\ u = -u - \lambda\,\Delta\,u &= 0, \quad \text{on } \partial\Omega, \end{aligned} \tag{A.1}$$

where we have assumed that non-homogeneous Dirichlet boundary conditions are replaced by an appropriate source term $f \in L^2(\Omega)$. The corresponding first-order system is:

$$\begin{aligned}
&\text{Find } (u, q, \mathbf{r}, \mathbf{t}) \text{ such that:} \\
&\qquad \nabla u - \mathbf{r} = \mathbf{0}, \quad \text{in } \Omega, \\
&-u - \lambda \nabla \cdot \mathbf{r} - q = 0, \quad \text{in } \Omega, \\
&\qquad \nabla q - \mathbf{t} = \mathbf{0}, \quad \text{in } \Omega, \\
&\qquad -D \nabla \cdot \mathbf{t} = -f, \quad \text{in } \Omega, \\
&\qquad u = 0, \quad \text{on } \partial\Omega, \\
&\qquad q = 0, \quad \text{on } \partial\Omega.
\end{aligned} \tag{A.2}$$

Multiplying this first-order system by test functions $(v, \mathbf{s}, w, \mathbf{p})$ and applying integration by parts to the terms $\nabla \cdot \mathbf{r}$ and $\nabla \cdot \mathbf{t}$ and a strong enforcement of boundary conditions yields the weak formulation:

$$\begin{aligned}
&\text{Find } (u, q, \mathbf{r}, \mathbf{t}) \in U^A(\Omega) \text{ such that:} \\
&\quad b((u, q, \mathbf{r}, \mathbf{t}), (v, w, \mathbf{s}, \mathbf{p})) = f(w), \quad \forall (v, w, \mathbf{s}, \mathbf{p}) \in V(\Omega),
\end{aligned} \tag{A.3}$$

where $U^A(\Omega) = V(\Omega) = H_0^1(\Omega) \times H_0^1(\Omega) \times [L^2(\Omega)]^2 \times [L^2(\Omega)]^2$ and:

$$\begin{aligned}
b((u, q, \mathbf{r}, \mathbf{t}), (v, w, \mathbf{s}, \mathbf{p})) &\overset{\text{def}}{=} \int_\Omega \left[(\nabla u - \mathbf{r}) \cdot \mathbf{s} + (\nabla q - \mathbf{t}) \cdot \mathbf{p} - (u + q) v + \lambda \mathbf{r} \cdot \nabla v + D \mathbf{t} \cdot \nabla w \right] \mathrm{d}\mathbf{x}, \\
f(w) &\overset{\text{def}}{=} \int_\Omega -f w \, \mathrm{d}\mathbf{x}.
\end{aligned} \tag{A.4}$$

By defining two bilinear forms:

$$\begin{aligned}
a((u, q, \mathbf{r}, \mathbf{t}), (v, w, \mathbf{s}, \mathbf{p})) &\overset{\text{def}}{=} -\int_\Omega \left[uv + qv + \mathbf{r} \cdot \mathbf{s} + \mathbf{t} \cdot \mathbf{p} \right] \mathrm{d}\mathbf{x}, \\
c((v, w), (\boldsymbol{\varepsilon}, \boldsymbol{\varphi})) &\overset{\text{def}}{=} \int_\Omega \boldsymbol{\varepsilon} \cdot \nabla v + \boldsymbol{\varphi} \cdot \nabla w \, \mathrm{d}\mathbf{x},
\end{aligned} \tag{A.5}$$

we can recast (A.4) as:

$$\begin{aligned}
&\text{Find } (u, q, \mathbf{r}, \mathbf{t}) \in U^A(\Omega) \text{ such that:} \\
&a((u, q, \mathbf{r}, \mathbf{t}), (v, w, \mathbf{s}, \mathbf{p})) + c((v, w), (\lambda \mathbf{r}, D \mathbf{t})) = f(w), \\
&\qquad\qquad\qquad\qquad\qquad\qquad\qquad\qquad \forall (v, w, \mathbf{s}, \mathbf{p}) \in V(\Omega). \\
&c((u, q), (\mathbf{s}, \mathbf{p})) \qquad\qquad\qquad\qquad = 0,
\end{aligned} \tag{A.6}$$

Proposition A.0.1. *Let $v \in H_0^1(\Omega)$. Then, $c_1(v, \boldsymbol{\varepsilon}) = \int_\Omega \boldsymbol{\varepsilon} \cdot \nabla v \, \mathrm{d}\mathbf{x}$ satisfies the inf-sup condition:*

$$\exists \gamma > 0 : \sup_{v \in H^1(\Omega)} \frac{|c_1(v, \boldsymbol{\varepsilon})|}{\|v\|_{H^1(\Omega)}} \geq \gamma \|\boldsymbol{\varepsilon}\|_{L^2(\Omega)} \tag{A.7}$$

Proof. Because $v \in H_0^1(\Omega)$ the Poincaré inequality gives:

$$\sup_{v \in H^1(\Omega)} \frac{|\int_\Omega \boldsymbol{\varepsilon} \cdot \nabla v \, \mathrm{d}\mathbf{x}|}{\|v\|_{H^1(\Omega)}} \geq \sup_{v \in H^1(\Omega)} \frac{|\int_\Omega \boldsymbol{\varepsilon} \cdot \nabla v \, \mathrm{d}\mathbf{x}|}{C \|\nabla v\|_{L^2(\Omega)}}.$$

Next, we pick $\nabla v = \boldsymbol{\varepsilon}$ to get:

$$\sup_{v \in H^1(\Omega)} \frac{|\int_\Omega \boldsymbol{\varepsilon} \cdot \nabla v \, \mathrm{d}\mathbf{x}|}{\|v\|_{H^1(\Omega)}} \geq \frac{|\int_\Omega \boldsymbol{\varepsilon} \cdot \boldsymbol{\varepsilon} \, \mathrm{d}\mathbf{x}|}{C \|\boldsymbol{\varepsilon}\|_{L^2(\Omega)}} = C \|\boldsymbol{\varepsilon}\|_{L^2(\Omega)},$$

and the proof is complete with $\gamma = C$. □

Lemma A.0.1. *Let* $(u, q, \mathbf{r}, \mathbf{t}) \in U(\Omega)$. *Then, the mixed weak problem* (A.6) *is well posed.*

Proof. Since the form $a(\cdot,\cdot)$ is clearly coercive, then the mixed problem (A.6) is well posed because all terms of $c(\cdot,\cdot)$ can be shown to satisfy an inf-sup condition shown in Proposition A.0.1, i.e., Brezzi's condition (See Theorem II.1.1 in [49]). □

Lemma A.0.1 leads to an inf-sup condition (see, e.g., [40]) of the form:

$$\exists \gamma > 0 : \sup_{(v,w,\mathbf{s},\mathbf{p})\in V(\Omega)} \frac{|b((u,q,\mathbf{r},\mathbf{t}),(v,w,\mathbf{s},\mathbf{p}))|}{\|(v,w,\mathbf{s},\mathbf{p})\|_{V(\Omega)}} \geq \gamma \, \|(u,q,\mathbf{r},\mathbf{t})\|_{U^A(\Omega)}. \tag{A.8}$$

Before showing the well-posedness of the AVS-FE weak formulation, let us use the continuous bilinear form $b(\cdot,\cdot)$ to write the corresponding AVS-FE weak form:

$$B((u,q,\mathbf{r},\mathbf{t}),(v,w,\mathbf{s},\mathbf{p})) = b((u,q,\mathbf{r},\mathbf{t}),(v,w,\mathbf{s},\mathbf{p})) + \langle D\,\mathbf{t}\cdot\mathbf{n}, w_m\rangle_{\Gamma_h} + \langle \lambda\,\mathbf{r}\cdot\mathbf{n}, v_m\rangle_{\Gamma_h}, \tag{A.9}$$

where $\langle D\,\mathbf{t}\cdot\mathbf{n}, w_m\rangle_{\Gamma_h} + \langle \lambda\,\mathbf{r}\cdot\mathbf{n}, v_m\rangle_{\Gamma_h} \overset{\text{def}}{=} \sum_{K_m\in\mathscr{P}_h} \oint_{\partial K_m} \{ D\,\gamma_{\mathbf{n}}^m(\mathbf{t})\,\gamma_0^m(w_m) + \lambda\,\gamma_{\mathbf{n}}^m(\mathbf{r})\,\gamma_0^m(v_m)\}\,\mathrm{d}s$. We also require the following intermediate results.

Proposition A.0.2. *Let* $\mathbf{t}, \mathbf{r} \in H(div, \mathscr{P}_h)$ *and* $v_m, w_m \in H^1(\mathscr{P}_h)$. *Then:*

$$\exists \gamma^s > 0 : \sup_{(v,w)\in H^1(\mathscr{P}_h)\times H^1(\mathscr{P}_h)} \frac{|\langle D\,\mathbf{t}\cdot\mathbf{n}, w_m\rangle_{\Gamma_h} + \langle \lambda\,\mathbf{r}\cdot\mathbf{n}, v_m\rangle_{\Gamma_h}|}{\|(v,w)\|_{H^1(\mathscr{P}_h)}} \geq \gamma^s \, \|(\mathbf{r},\mathbf{t})\|_{\hat{U}(\Gamma_h)}, \tag{A.10}$$

where $H(div, \mathscr{P}_h)$ *denotes the broken* $H(div)$ *space and* $\|(\mathbf{r},\mathbf{t})\|_{\hat{U}(\Gamma_h)}$ *is the minimum energy extension norm:*

$$\|(\mathbf{r},\mathbf{t})\|_{\hat{U}(\Gamma_h)} \overset{def}{=} \sum_{K_m\in\mathscr{P}_h} \oint_{\partial K_m} \{\gamma_{\mathbf{n}}^m(\mathbf{t})\,\gamma_0^m(w_m) + \gamma_{\mathbf{n}}^m(\mathbf{r})\,\gamma_0^m(v_m)\}\,\mathrm{d}s = \inf(\|\mathbf{r}\|^2_{\mathrm{H}(div,\Omega)} + \|\mathbf{t}\|^2_{\mathrm{H}(div,\Omega)})^{1/2} \tag{A.11}$$

Proof. See Theorem 2.3 in [48]. □

Proposition A.0.3. *Let* $\mathbf{t}, \mathbf{r} \in H(div, \Omega)$ *and* $v_m, w_m \in H^1(\mathscr{P}_h)$. *Then:*

$$\langle D\,\mathbf{t}\cdot\mathbf{n}, w_m\rangle_{\Gamma_h} + \langle \lambda\,\mathbf{r}\cdot\mathbf{n}, v_m\rangle_{\Gamma_h} = 0, \quad \forall v_m, w_m \in H^1(\Omega). \tag{A.12}$$

Proof. Since functions in $H(\mathrm{div}, \Omega)$ have zero jump across mesh interfaces both terms must vanish for all single valued functions v_m and w_m on Γ_h, see Theorem 2.3 in [48]. □

Now, Lemma A.0.1 and Propositions A.0.2 and A.0.3 correspond to the necessary assumptions of Theorem 3.3 in [48]. Hence, we replicate their arguments to show the following assertion:

Lemma A.0.2. *Let* $(u, q, \mathbf{r}, \mathbf{t}) \in U(\Omega)$. *Then, the AVS-FE weak formulation* (A.9) *is well posed.*

Proof. Since continuity of the bilinear form and linear functional can be shown in a straightforward manner by the Cahchy-Schwarz inequality and successive integration by parts. The inf-sup condition is the last required point of the Babuška Lax-Milgram Theorem [47] for the well-posedness of the weak formulation. By (A.8) we have:

$$C\,\|(u,q,\mathbf{r},\mathbf{t})\|_{U^A(\Omega)} \leq \sup_{(v,w,\mathbf{s},\mathbf{p})\in V(\Omega)} \frac{|b((u,q,\mathbf{r},\mathbf{t}),(v,w,\mathbf{s},\mathbf{p}))|}{\|(v,w,\mathbf{s},\mathbf{p})\|_V},$$

notice that in the denominator we have replaced $\|(v,w,\mathbf{s},\mathbf{p})\|_{V(\Omega)}$ with $\|(v,w,\mathbf{s},\mathbf{p})\|_V$, which are equivalent for functions $(v,w,\mathbf{s},\mathbf{p}) \in V(\Omega)$. We then add the duality pairings, i.e., zero (see Proposition A.0.3) in the numerator:

$$C\,\|(u,q,\mathbf{r},\mathbf{t})\|_{U^A(\Omega)} \leq \sup_{(v,w,\mathbf{s},\mathbf{p})\in V(\Omega)} \frac{|b((u,q,\mathbf{r},\mathbf{t}),(v,w,\mathbf{s},\mathbf{p})) + \langle D\,\mathbf{t}\cdot\mathbf{n}, w_m\rangle_{\Gamma_h} + \langle \lambda\,\mathbf{r}\cdot\mathbf{n}, v_m\rangle_{\Gamma_h}|}{\|(v,w,\mathbf{s},\mathbf{p})\|_V},$$

finally, we test with a larger space $V(\mathscr{P}_h) \supset V(\Omega)$ to establish the inf-sup condition:

$$C\,\|(u,q,\mathbf{r},\mathbf{t})\|_{U^A(\Omega)} \leq \sup_{(v,w,\mathbf{s},\mathbf{p})\in V(\mathscr{P}_h)} \frac{|B((u,q,\mathbf{r},\mathbf{t}),(v,w,\mathbf{s},\mathbf{p}))|}{\|(v,w,\mathbf{s},\mathbf{p})\|_{V(\mathscr{P}_h)}}. \tag{A.13}$$

Next, by Proposition A.0.2:

$$\gamma^s \|(\mathbf{r},\mathbf{t})\|_{\hat{U}(\Gamma_h)} \leq \sup_{(v,w,\mathbf{s},\mathbf{p})\in V(\mathscr{P}_h)} \frac{|\langle D\,\mathbf{t}\cdot\mathbf{n}, w_m\rangle_{\Gamma_h} + \langle \lambda\,\mathbf{r}\cdot\mathbf{n}, v_m\rangle_{\Gamma_h}|}{\|(v,w,\mathbf{s},\mathbf{p})\|_V}.$$

By (A.9), we get:

$$\gamma^s \|(\mathbf{r},\mathbf{t})\|_{\hat{U}(\Gamma_h)} \leq \sup_{(v,w,\mathbf{s},\mathbf{p})\in V(\mathscr{P}_h)} \frac{|B((u,q,\mathbf{r},\mathbf{t}),(v,w,\mathbf{s},\mathbf{p})) - b((u,q,\mathbf{r},\mathbf{t}),(v,w,\mathbf{s},\mathbf{p}))|}{\|(v,w,\mathbf{s},\mathbf{p})\|_V},$$

which can be further bound using (A.8):

$$\gamma^s \|(\mathbf{r},\mathbf{t})\|_{\hat{U}(\Gamma_h)} \leq \gamma \|(u,q,\mathbf{r},\mathbf{t})\|_{U^A(\Omega)} + \sup_{(v,w,\mathbf{s},\mathbf{p})\in V(\mathscr{P}_h)} \frac{|B((u,q,\mathbf{r},\mathbf{t}),(v,w,\mathbf{s},\mathbf{p}))|}{\|(v,w,\mathbf{s},\mathbf{p})\|_V},$$

where the first term in the RHS can be bound by (A.13). Finally, we note that the norm on $U(\Omega)$ can be expressed as:

$$\|(u,q,\mathbf{r},\mathbf{t})\|^2_{U(\Omega)} = \|(\mathbf{r},\mathbf{t})\|^2_{\hat{U}(\Gamma_h)} + \|(u,q,\mathbf{r},\mathbf{t})\|^2_{U^A(\Omega)},$$

leading to the desired *inf-sup* condition:

$$C\,\|(u,q,\mathbf{r},\mathbf{t})\|_{U(\Omega)} \leq \sup_{(v,w,\mathbf{s},\mathbf{p})\in V(\mathscr{P}_h)} \frac{|B((u,q,\mathbf{r},\mathbf{t}),(v,w,\mathbf{s},\mathbf{p}))|}{\|(v,w,\mathbf{s},\mathbf{p})\|_{V(\mathscr{P}_h)}}. \quad \square \tag{A.14}$$

References

[1] T. Wisdom, Recent developments in tailings dewatering technology, presented at the Society for Mining, in: Metallurgy and Exploration Annual Meeting, February 26, Phoenix, AZ, 2020.
[2] C.M. Elliott, Z. Songmu, On the Cahn-Hilliard equation, Arch. Ration. Mech. Anal. 96 (4) (1986) 339–357.
[3] J.T. Oden, Finite Elements of Nonlinear Continua, Courier Corporation, 2006.
[4] R. Courant, K. Friedrichs, H. Lewy, Über die partiellen differenzengleichungen der mathematischen physik, Math. Ann. 100 (1) (1928) 32–74.
[5] F. Chave, D.A. Di Pietro, F. Marche, F. Pigeonneau, A hybrid high-order method for the Cahn-Hilliard problem in mixed form, SIAM J. Numer. Anal. 54 (3) (2016) 1873–1898.
[6] S. Clavijo, A. Sarmiento, L. Espath, L. Dalcin, A. Cortes, V.M. Calo, Reactive n-species Cahn-Hilliard system: a thermodynamically-consistent model for reversible chemical reactions, J. Comput. Appl. Math. 350 (2019) 143–154.
[7] G.N. Wells, E. Kuhl, K. Garikipati, A discontinuous Galerkin method for the Cahn-Hilliard equation, J. Comput. Phys. 218 (2) (2006) 860–877.
[8] J.W. Barrett, J.F. Blowey, H. Garcke, On fully practical finite element approximations of degenerate Cahn-Hilliard systems, ESAIM: Math. Model. Numer. Anal. 35 (4) (2001) 713–748.
[9] H. Gómez, V.M. Calo, Y. Bazilevs, T.J. Hughes, Isogeometric analysis of the Cahn-Hilliard phase-field model, Comput. Methods Appl. Mech. Eng. 197 (49–50) (2008) 4333–4352.
[10] M. Fernandino, C. Dorao, The least squares spectral element method for the Cahn-Hilliard equation, Appl. Math. Model. 35 (2) (2011) 797–806.
[11] E. Dean, R. Glowinski, D. Trevas, An approximate factorization/least squares solution method for a mixed finite element approximation of the Cahn-Hilliard equation, Jpn. J. Ind. Appl. Math. 13 (3) (1996) 495.
[12] T.J.R. Hughes, J.R. Stewart, A space-time formulation for multiscale phenomena, J. Comput. Appl. Math. 74 (1996) 217–229.
[13] T.J. Hughes, G.M. Hulbert, Space-time finite element methods for elastodynamics: formulations and error estimates, Comput. Methods Appl. Mech. Eng. 66 (3) (1988) 339–363.
[14] A.K. Aziz, P. Monk, Continuous finite elements in space and time for the heat equation, Math. Comput. 52 (186) (1989) 255–274.
[15] T.E. Ellis, L. Demkowicz, J. Chan, R.D. Moser, Space-time DPG: Designing a method for massively parallel CFD, ICES report 14-32, The Institute for Computational Engineering and Sciences, The University of Texas at Austin, 2014.
[16] T. Ellis, J. Chan, L. Demkowicz, Robust DPG methods for transient convection-diffusion, in: Building Bridges: Connections and Challenges in Modern Approaches to Numerical Partial Differential Equations, Springer, 2016, pp. 179–203.
[17] N.V. Roberts, L. Demkowicz, R. Moser, A discontinuous Petrov–Galerkin methodology for adaptive solutions to the incompressible Navier–Stokes equations, J. Comput. Phys. 301 (2015) 456–483.
[18] P.B. Bochev, M.D. Gunzburger, Least-Squares Finite Element Methods, vol. 166, Springer Science & Business Media, 2009.
[19] V.M. Calo, A. Romkes, E. Valseth, Automatic variationally stable analysis for FE computations: an introduction, in: G. Barrenechea, J. Mackenzie (Eds.), Boundary and Interior Layers, Computational and Asymptotic Methods BAIL 2018, Springer, 2020, pp. 19–43.
[20] L. Demkowicz, J. Gopalakrishnan, A class of discontinuous Petrov-Galerkin methods. Part I: the transport equation, Comput. Methods Appl. Mech. Eng. 199 (23) (2010) 1558–1572.
[21] V.M. Calo, A. Ern, I. Muga, S. Rojas, An adaptive stabilized conforming finite element method via residual minimization on dual discontinuous Galerkin norms, Comput. Methods Appl. Mech. Eng. 363 (2020) 112891.
[22] C. Carstensen, P. Bringmann, F. Hellwig, P. Wriggers, Nonlinear discontinuous Petrov–Galerkin methods, Numer. Math. 139 (3) (2018) 529–561.
[23] J.W. Cahn, J.E. Hilliard, Free energy of a nonuniform system. I. Interfacial free energy, J. Chem. Phys. 28 (2) (1958) 258–267.
[24] C. Carstensen, L. Demkowicz, J. Gopalakrishnan, A posteriori error control for DPG methods, SIAM J. Numer. Anal. 52 (3) (2014) 1335–1353.
[25] L. Demkowicz, J. Gopalakrishnan, Analysis of the DPG method for the Poisson equation, SIAM J. Numer. Anal. 49 (5) (2011) 1788–1809.
[26] L. Demkowicz, J. Gopalakrishnan, A class of discontinuous Petrov-Galerkin methods. II. Optimal test functions, Numer. Methods Partial Differ. Equ. 27 (1) (2011) 70–105.
[27] L. Demkowicz, J. Gopalakrishnan, A class of discontinuous Petrov-Galerkin methods. Part III: adaptivity, Appl. Numer. Math. 62 (4) (2012) 396–427.
[28] S. Nagaraj, S. Petrides, L.F. Demkowicz, Construction of DPG Fortin operators for second order problems, Comput. Math. Appl. 74 (8) (2017) 1964–1980.
[29] L.F. Demkowicz, J. Gopalakrishnan, An overview of the discontinuous Petrov Galerkin method, in: Recent Developments in Discontinuous Galerkin Finite Element Methods for Partial Differential Equations, Springer, 2014, pp. 149–180.

[30] M. Woźniak, M. Łoś, M. Paszyński, L. Demkowicz, Fast parallel integration for three dimensional discontinuous Petrov Galerkin method, Proc. Comput. Sci. 101 (2016) 8–17.
[31] N.V. Roberts, T. Bui-Thanh, L. Demkowicz, The DPG method for the Stokes problem, Comput. Math. Appl. 67 (4) (2014) 966–995.
[32] A. Cohen, W. Dahmen, G. Welper, Adaptivity and variational stabilization for convection-diffusion equations, ESAIM: Math. Model. Numer. Anal. 46 (5) (2012) 1247–1273.
[33] F. Rathgeber, D.A. Ham, L. Mitchell, M. Lange, F. Luporini, A.T. McRae, G.-T. Bercea, P.H. Markall, R. Graham, Kelly, Firedrake: automating the finite element method by composing abstractions, ACM Trans. Math. Softw. 43 (3) (2017) 24.
[34] M.S. Alnæs, J. Blechta, J. Hake, A. Johansson, B. Kehlet, A. Logg, C. Richardson, J. Ring, M.E. Rognes, G.N. Wells, The FEnics project version 1.5, Arch. Numer. Softw. 3 (100) (2015) 9–23.
[35] V. Girault, P.-A. Raviart, Finite element methods for Navier-Stokes equations; theory and algorithms, in: Springer Series in Computational Mathematics, vol. 5, Springer-Verlag, 1986.
[36] S. Abhyankar, J. Brown, E.M. Constantinescu, D. Ghosh, B.F. Smith, H. Zhang, Petsc/ts: a modern scalable ode/dae solver library, arXiv preprint, arXiv: 1806.01437, 2018.
[37] S. Balay, S. Abhyankar, M.F. Adams, J. Brown, P. Brune, K. Buschelman, L. Dalcin, A. Dener, V. Eijkhout, W.D. Gropp, D. Karpeyev, D. Kaushik, M.G. Knepley, D.A. May, L.C. McInnes, R.T. Mills, T. Munson, K. Rupp, P. Sanan, B.F. Smith, S. Zampini, H. Zhang, H. Zhang, PETSc users manual, Tech. Rep. ANL-95/11 - Revision 3.12, Argonne National Laboratory, 2019, https://www.mcs.anl.gov/petsc.
[38] K.G. Van Der Zee, J. Tinsley Oden, S. Prudhomme, A. Hawkins-Daarud, Goal-oriented error estimation for Cahn-Hilliard models of binary phase transition, Numer. Methods Partial Differ. Equ. 27 (1) (2011) 160–196.
[39] M. Kästner, P. Metsch, R. De Borst, Isogeometric analysis of the Cahn-Hilliard equation-a convergence study, J. Comput. Phys. 305 (2016) 360–371.
[40] L. Demkowicz, P. Zanotti, Construction of DPG Fortin operators revisited, Comput. Math. Appl. (2020).
[41] W. Dörfler, A convergent adaptive algorithm for Poisson's equation, SIAM J. Numer. Anal. 33 (3) (1996) 1106–1124.
[42] L. Goudenège, D. Martin, G. Vial, High order finite element calculations for the Cahn-Hilliard equation, J. Sci. Comput. 52 (2) (2012) 294–321.
[43] S.C. Brenner, A.E. Diegel, L.-Y. Sung, A robust solver for a second order mixed finite element method for the Cahn-Hilliard equation, J. Comput. Appl. Math. 364 (2020) 112322.
[44] Q. Deng, P. Behnoudfar, V.M. Calo, High-order generalized-α methods, arXiv preprint, arXiv:1902.05253, 2019.
[45] J. Chung, G. Hulbert, A time integration algorithm for structural dynamics with improved numerical dissipation: the generalized-α method, J. Appl. Mech. 60 (2) (1993) 371–375.
[46] N.V. Roberts, Camellia: a rapid development framework for finite element solvers, Comput. Methods Appl. Math. 19 (3) (2019) 581–602.
[47] I. Babuška, Error-bounds for finite element method, Numer. Math. 16 (1971) 322–333.
[48] C. Carstensen, L. Demkowicz, J. Gopalakrishnan, Breaking spaces and forms for the DPG method and applications including Maxwell equations, Comput. Math. Appl. 72 (3) (2016) 494–522.
[49] F. Brezzi, M. Fortin, Mixed and Hybrid Finite Element Methods, vol. 15, Springer-Verlag, 1991.